Mechanical and Deformation Properties of Rubberized Engineered Cementitious Composites (ECC) Containing 3D-Printed Origami Hollow Bodies

JOSHUA CHOO LEY ERN

17006141

Dissertation submitted in partial fulfilment of

the requirements for the

Bachelor of Civil Engineering with Honours

JANUARY 2022

Universiti Teknologi PETRONAS

32610 Seri Iskandar

Perak Darul Ridzuan

CERTIFICATION OF APPROVAL

Mechanical and Deformation Properties of Rubberized Engineered Cementitious Composites (ECC) Containing 3D-Printed Origami Hollow Bodies

by

Joshua Choo Ley Ern
17006141

A project dissertation submitted to the
Civil Engineering Programme
Universiti Teknologi PETRONAS
in partial fulfilment of the requirement for the
BACHELOR OF CIVIL ENGINEERING WITH HONOURS

Approved by,

ASSOC. PROF. IR. DR. BASHAR S MOHAMMED
Chair
Civil & Environmental Engineering Department
Universiti Teknologi PETRONAS
32610 Seri Iskandar
Perak Darul Ridzuan, Malaysia

(Assoc. Prof. Ir. Dr. Bashar S Mohammed)

UNIVERSITI TEKNOLOGI PETRONAS
SERI ISKANDAR, PERAK
January 2022

CERTIFICATION OF ORIGINALITY

This is to certify that I am responsible for the work submitted in this project, that the original work is my own except as specified in the references and acknowledgements, and that the original work contained herein have not been undertaken or done by unspecified sources or persons.

JOSHUA CHOO LEY ERN

ABSTRACT

Bubble concrete is a lightweight concrete achieved by mixing high-strength hollow bodies into concrete. Bubble concrete is different from the biaxial voided slabs as it can reduce the density of concrete while ensuring the strength. The hollow bodies used not only to create multiple cavities, but also to transfer internal stresses. Several studies were done on the randomly mixed circular and concave steel hollow bodies in concrete where it reported the shape and material of the hollow bodies significantly affect the strength of the bubble concrete. This work reports the finding of an experimental investigation on the use of origami shape hollow bodies. In the present study, 3D-Printed origami shape hollow bodies held in fixed position are used to mix in Rubberized Engineered Cementitious Composites (ECC) to form multiple cavities. The research was performed by utilizing the response surface methodology (RSM) and development of response models to predict the density, compressive strength, modulus of elasticity and Poisson's ratio of the bubble concrete. The mechanical, deformation properties and failure mode of 3D-Printed origami hollow bodies mixed in Rubberized ECC are being investigated. The results show that the mechanical and deformation properties of the Rubberized ECC were negatively affected by the increased number of 3D-Printed origami hollow bodies. Experimental results indicate that the Rubberized ECC containing 3D-Printed origami hollow bodies can reduce its density to 1.886 g/cm^3 – 1.921g/cm^3 (94.5%-96.2%, compared to control Rubberized ECC), its average compressive strength reaches 28.55 MPa, Modulus of Elasticity and Poisson's ratio of 14.31 GPa and 0.21 respectively. Optimization was carried out which has the desirability value of 0.835. Nine number of origami hollow bodies with 20 mm spacing are found to yield optimum mechanical and deformation properties.

ACKNOWLEDGEMENT

First and foremost, I would like to give my upmost appreciation to my Final Year Project (FYP) supervisor, Assoc. Prof. Dr Bashar S. Mohammed who open heartedly accepted me under his wings for my FYP. He has provided me the guidance and endless support throughout the project period. Heartiest thanks for his continuous encouragement and motivation in keeping in track of me to complete the FYP within the timeline given. With his immense knowledge in research of concrete, he has enlightened my way in my project. Moving on, I would like to thank my FYP course coordinator, Dr Lavania Baloo for guiding me through frequent updates regarding the project timeline and arranging adjunct lectures for my better understanding on my project.

Next, I would like to take this opportunity to thank Mr. Isyaka Abdulkadir for assisting me to complete my laboratory work for my FYP. He has been great mentor for me throughout the project duration. His ceaseless support and guidance gave me the courage to move on to completing this dissertation.

Apart from that, I would like to express my gratitude to the technicians at the concrete laboratory of Universiti Teknologi PETRONAS, Mr. Johan Ariff and Mrs. Intan, who have provided the technical support and facilitated me during the experimental work. I am grateful and would like thank course mates who have assisted me at the concrete laboratory.

Last but not the least, I would like to thank my parents and family, whose unlimited love and support gave me the courage and patience to undertake this challenging task. Special thanks to Universiti Teknologi PETRONAS for providing good lab facilities so that I can complete my laboratory work smoothly.

TABLE OF CONTENT

LIST OF TABLES

LIST OF FIGURES

CHAPTER 1

INTRODUCTION

1.1 Background Study

Weight reduction in civil engineering and building structures are very effective in reducing seismic force and ensuring safety and habitability, therefore weight reduction in structural materials especially concrete remains an important issue. Lightweight concrete is known by low density, good seismic performance and excellent thermal insulation which making it an increasingly popular building structure material around the world. Light aggregate concrete is considered one of the most typical types of lightweight concrete, which have been the subject of numerous studies [1-7]. The light aggregates used in lightweight concrete are commonly expanded shale, clay or slate materials fired in rotary kiln to develop a porous structure. Other materials are also used such as air-cooled blast furnace slag and perlite. Materials like clay, perlite or vermiculite are convenient starting materials to produce lightweight aggregate concrete. A foaming process produces a well-known lightweight aggregate with a very low apparent density and closed porosity made from glass [8].

In the previous studies, Professor Pei-Shan Chen invented a new type of lightweight concrete inspired by hollow bird bones, which is formed by mixing the high-strength hollow bodies into concrete, named it bubble concrete [9-10]. The bubble concrete is different from foamed concrete and biaxial voided concrete slabs [11-12] because the hollow bodies are used not only to create multiple cavities, but also to transfer internal stresses. By taking advantages of the shape characteristics and adhesion performance of the hollow body with concrete, the weight is reduced while maintaining and improving the strength and rigidity of the concrete. Figure 1.1 shows a schematic diagram of bubble concrete.

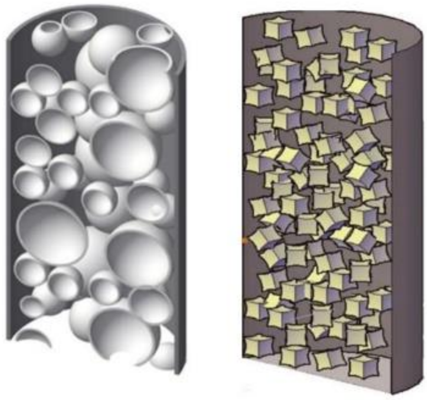

FIGURE 1.1: Bubble Concrete with High-Strength Hollow Bodies [9]

Numerous Studies on random mix of metallic hollow sphere are proposed and attracting attention [10]. It can be said that the method of reducing density of the concrete by forming microcavities inside the concrete is common in the material weight reduction technology. The author proposed a new method of reducing the weight of concrete by fixing the position of origami shape hollow bodies in the concrete. Bubble concrete significantly reduce the density of concrete, improve thermal insulation performance, and reduce the seismic load impact on concrete structure while maintaining the compressive strength and modulus elasticity of concrete. This is a revolutionary lightweight concrete solution, Professor Pei-Shan Chen have attempted to apply it to other fields such as shipbuilding, metal materials, aerospace materials, etc. Figure 1.2 shows the inspiration of bubble concrete.

Engineered Cementitious Composite (ECC) is a unique sort of cement mixture that contains a unique composition of low volume fibres and various composites to provide excellent ductility, tensile strength, and repairability. Because traditional concrete and fibre reinforced concrete are fragile, they shatter easily under climatic and mechanical pressures, reducing construction durability. Efforts to change the brittle nature of conventional concrete brings in the invention of ECCs, which have a wide range of environmental durability, minimal embodied energy, and a negative carbon footprint, making them an environmentally friendly construction material with self–healing capability. ECCs have a narrow crack width, and the development of these cracks improves the ability of ECCs to withstand the effects of hot, frosty, and damp climatic conditions, in addition to their low permeability.

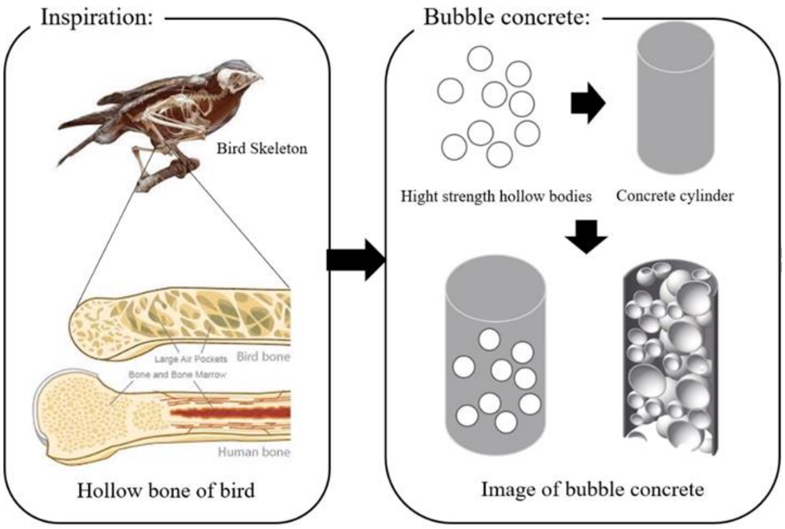

FIGURE 1.2: Inspiration of Bubble Concrete from Hollow Bone of Bird [9]

1.2 Problem Statement

Reducing the density of concrete can reduce the impact of seismic loads on the structure, so there is a need to study lightweight concrete technology. Finding the suitable method to reduce the density of concrete and guarantee the strength is also lacking prior to the bubble concrete. Pioneering research has been carried out on novel lightweight concrete material. In the previous studies, authors studied about the bubble concrete with different materials and results showed that the shape and position of the hollow bodies would affect the compressive strength and stress distribution of the bubble concrete. Steel-made spherical and concave hollow bodies were used in the bubble concrete to study the strength and Young’s modulus of the bubble concrete. Currently, it is still in the early stages of researching on bubble concrete and there is a need to study of different shapes of hollow bodies on the properties of Engineered Cementitious Composites (ECC) properties. Consequently, a suitable hollow body model can be found to enhance the concrete performance. However, the studies and research on fixed position origami hollow bodies in ECC are lacking.

1.3 Aim and Objectives

The aim of this research is to access the density and mechanical properties of Rubberized Engineered Cementitious Composites with fixed position origami hollow bodies. Response surface models and optimization of the mixes will be developed.

1. To investigate the effect of fixed position origami hollow bodies on the density, mechanical and deformation properties of the Rubberized ECC.
2. To develop response surface models and carry out optimization on the effect of origami hollow bodies on the Rubberized ECC.

1.4 Scope of Research

This research covers the determination of the density and mechanical properties of bubble concrete with fixed position origami hollow bodies. It also covers the development of response surface models for the compressive strength, modulus of elasticity and Poisson's ratio of the concrete. Rubberized-Engineered Cementitious Composites (ECC) will be used for the mix design. Thirteen number of mixes were generated using the central composite design (CCD) option of response surface methodology (RSM). The developed mixes contain varying combinations and level of the input variables that are spacing between fixed origami hollow bodies and number of origami hollow bodies at 10mm – 20mm and 9 – 21 respectively. Compressive strength test, modulus of elasticity and Poisson's ratio test were carried out at 28 days of curing. From the results, the influence of the different levels and combination of the input factor on the properties of the concrete was discussed and analysed. Response models for the mechanical properties of the concrete will be developed and analysed by using ANOVA analysis. Finally, an optimization was performed to obtain the optimum levels of variables on the effect of the bubble concrete. Failure mode of the bubble concrete will be discussed based on observation.

CHAPTER 2

LITERATURE REVIEW

2.1 Development of Engineered Cementitious Composites (ECC)

The materials used to construct structures have a significant impact on their performance. There are demands and problems of designing new structural systems such taller buildings, bridge deck link slabs, and longer span bridges. Pavement systems are in the high need for endurance, as well as repairs to existing civil infrastructure. High-performance civil engineering materials are required for infrastructure systems. Material qualities such as high strength, stiffness, ductility, and elasticity are important factors.

When exposed to tension, cementitious materials including concrete have brittle behaviour as well as limited tensile strength and strain capacity. This brittle behaviour has restricted ECC's wide application due to its negative effect on structural performance in respect to ductility when under tension and shear, as well as durability. To address the brittleness of cementitious materials, short, discrete high-strength fiber distributed randomly were incorporated into the cementitious matrix. The incorporation of fiber is an old idea which was practiced in ancient China and Egypt 3500-4500 years ago. The idea sprang up again in the late 1960s, as the normal fiber reinforced cementitious composites (FRCCs) generally displays strain-softening behaviour when subjected to tension, with single wide crack openings. Nevertheless, the toughness of the material reinforced with short fiber is tremendously increased, though, the strain capacity of FRCCs is still low compared to normal unreinforced concrete. Furthermore, the workability unavoidably deteriorates because of fiber addition [13].

ECCs are a new generation of HPFRCCs that utilize as little as 2% volume fraction of fiber and strain in the range of 3-7% with a tight crack width of about 60 µm [14-16]. The ECC is designed based on the principles of micromechanics through the system tailoring of materials to achieve a fundamental metal-like behavior when subjected to tensile tests. Like conventional HPFRCCs, the constituent materials of the ECC are short discrete fibers, cementitious materials, fine aggregates, water and high range water reducer (HRWR). Unlike the conventional HPFRCC, such as slurry infiltrated fiber concrete (SIFCON), which uses high-volume fiber to achieve high performance, the ECC utilizes a low volume of fiber [17]. The low fiber used to achieve high performance in ECCs indicates compliance of the economic requirement of the material. The fibers are tailored to work with the matrix to ensure localized brittle failure is restrained, assuring the distribution of uniform micro-crack propagation. The slip hardening of fibers ensures the ECC can handle additional increasing loads that promote new crack formation at other locations [18]. The ECC demonstrates high ductility at low fiber volume fractions with tensile strain in the range of 3-7% and a tight crack width of about 60 µm [14]. Furthermore, 13 in respect to applied load, the crack width in ECCs hardly exceeds 100 µm [19]. The engineering of the ECC material is based on the pattern of the connection between processing, material properties, microstructure of the material, and performance, in which the link between the mechanical performance of the composites and microstructure is the micromechanics. The developed micromechanics principles serve as guide to tailor the constituents of the composites including the fiber, matrix, and interface to achieve the overall performance of the structure. This has taken the material design from trial-and-error to a systematic and "engineered" selection combination of materials "engineered" selection. In that sense, micromechanics is the guiding principle of ECC development. The principle aim of the design of the ECC is achieving a material with pseudo strain-hardening behavior after the initiation of first cracking. This entails increasing the toughness of the material at failure.

2.2 Rubberized-Engineered Cementitious Composites

As construction technology leans towards environmental sustenance and green engineering, scientists and engineers alike move towards finding plausible alternatives to produce technology that not only serves its purpose but also complies with stringent environmental regulations. Incorporating crumb rubber from old tyres into concrete mixes could go a long way environmentally as it works best compared to other tyre disposal methods. Many types of research involving the incorporation of crumb rubber into concrete mixes have been undertaken. The addition of crumb rubber as a replacement to fine aggregates cardinally reduces the strength and stiffness of the concrete [20]. However, the composites still meet all structural requirements and show a decrease in density and an increase in drying shrinkage. It has also indicated enhanced toughness as well as ductility. In another study, crumb rubber and lightweight scoria aggregate was used in replacement of normal aggregates to produce light weight self-compacting concrete. Inclusion of polypropylene and steel fibres improves the strength properties and benefits in resisting the strength loss when exposed to elevated temperature, while scarifying the workability [21]. Similarly, addition of crumb rubber to concrete can also provide freeze-thaw protection while causes about 5.24 % loss in 28 days compressive strength.

2.3 Fundamental Principle of Hollow Bodies in Bubble Concrete

Cavities in lightweight concrete reduce the effective cross-sectional area for internal stress transfer under normal circumstances. Furthermore, when the concrete is stressed, multiple cavities can cause concrete to crack, thus lowering concrete's strength. The high strength hollow bodies in the bubble concrete, on the other hand, can provide an effective cross-sectional area for stress transmission [22]. Furthermore, contact between bubble concrete and hollow bodies can give adhesion and prevent the concrete from failing prematurely.

The shape and material adhesion of the hollow bodies have a significant impact on the strength of the bubble concrete. As a result, numerous hollow body shapes have been studied, as shown in Figure 2.1. Among all the hollow bodies, Figure 2.1a indicates the roughening surface of the hollow bodies to improve the adhesion between the concrete and the hollow bodies. Figure 2.1b shows inner concave shape which can reduce the lateral expansion of the hollow bodies, and Figure 2.1c illustrates the hollow bodies with wires and/or ribs to increase compressive strength.

In the previous studies, spherical hollow bodies were mainly used. The spherical hollow bodies will expand in all directions under compression, resulting in a reduction in the ultimate strength of the bubble concrete [9]. Research on randomly mixed hollow bodies have been done and results shows that hollow bodies that are compressed vertically expand in an oblique direction. The stress distribution varies with the number of hollow bodies due to the random position of the hollow bodies. The stress is superimposed in area with significant number of hollow bodies. The stress is close to the loading value in an area with a modest number of hollow bodies. In addition, steel-made spherical and concave hollow bodies were used in the bubble concrete and because the steel surface are mild, there is inadequate adhesion between the concrete and hollow bodies therefore concrete cannot provide enough internal tension to keep the external concrete from peeling off. To tackle this difficulty, origami hollow bodies are used in this concurrent investigation. When compressive stresses are applied to the origami concave body, its unique form mechanism produces inward compression, reducing the extrusion of the hollow bodies into surrounding concrete [22]. The origami model is yet to be investigated on the mechanical and deformation properties of the bubble concrete.

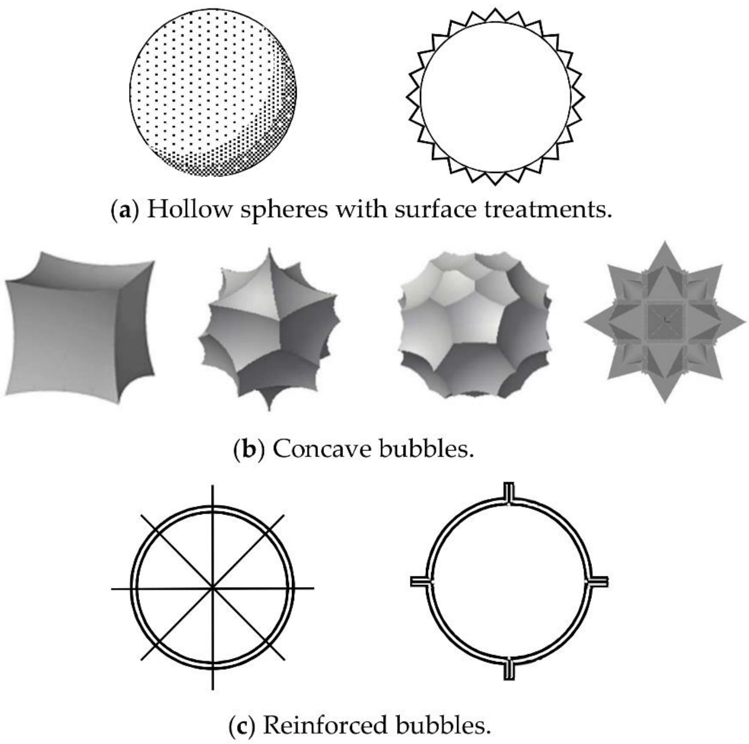

FIGURE 2.1: Hollow Bodies with Different Shapes and Mechanisms

2.4 Response Surface Methodology

RSM is a graphical representation of the responses obtained using one or more variables during mathematical and statistical procedures to model responses. A polynomial equation defined by a regression analysis is usually used to represent the relationship between the input variables and output response [23]. In concrete technologies, variables include the mixture of ingredients, and the responses are the desired concrete properties. An analysis of such a response consists of the collection of experimental data, the selection of a suitable model that fits the data, and a diagnosis of the suitability of the fitted model. A graphical response provides an opportunity to visually determine the independent variables influencing the system. Once the influential variables are identified, an approximate solution of the response is obtained. To optimize the experimental variables, a model must be developed. The optimization of the response surface is conducted to find the best solution for the response. Such a model is a prerequisite to obtaining an optimized general solution to the problem. Building such a model requires experimental data [24].

In multi-objective optimization, several responses are considered at the same time to find optimal compromises among the total number of responses considered at the that moment. The desirability function is the most important and considered multicriteria methods adopted in optimization [25, 26]. The desirability function for individual responses is assigned through criteria that each response must fulfil in the measuring procedure. Afterwards, the overall desirability, D utilizing desirability of 37 individual responses is obtained. The overall scale of desirability is between 0 and 1, for completely undesirable and fully desirable responses, respectively [25]. The desirability application in multiple response optimization procedures brings merits such as economy, efficiency, and objectivity. With these outline advantages, the application of multi-objective optimization in ECC will harness a lot of benefits. The purpose of multi-objective optimization is to simultaneously optimize the levels of variables to achieve a desired performance for a system.

Several researchers have utilized RSM and optimization techniques in concrete technology to develop models illustrating the relationships between responses (properties) and variables (factors). Savastano et al. [27] investigated the effects of three variables (water–cement ratio, tensile strength of steel fiber, and fiber volume fraction) to develop a ductile FRC with the desired fracture energy and splitting tensile strength. Bayramov et al. [28] investigated the effects of the fiber aspect ratio (l/d) and fiber volume fraction on the fracture energy and splitting tensile strength of FRC. They maximized the fracture energy and splitting tensile strength, while minimizing the fiber volume and reducing cost.

2.5 Summary

The application of RSM to develop models for the responses of ECC materials and the utilization of multi-objective optimization to achieve desired properties of ECCs for specific applications has been unavailable until now. ECC are a new class of HPFRCCs, and their application in the construction industry has been limited to repair/retrofitting and as structural elements in structures. Their application as a solo structural element has been restricted due to their low values of modulus of elasticity. The application of ECCs as a repair/retrofitting material has also generated some concerns from researchers due to their high shrinkage values.

The literature review stated that many types of research involving the incorporation of crumb rubber into concrete mixes have been undertaken. The addition of crumb rubber as a replacement to fine aggregates cardinally reduces the strength and stiffness of the concrete and as construction technology it leans towards environmental sustenance and green engineering. Rubberized Engineered Cementitious Composites (ECC) will be used in this research. There is still needed to source materials that will improve the performance of ECCs to widen its application in the construction industry. It is important to apply RSM to develop response models and to apply multi-objective optimization technique that has the capability to achieve desired specified properties within the design of the materials.

CHAPTER 3

METHODOLOGY

3.1 Introduction

This chapter contains details of experimental program conducted for the purpose of investigating the mechanical and deformation properties of Rubberized Engineered Cementitious Composites (ECC) containing 3D Origami Hollow Aggregate. The methodology consists of two parts. The first part is the experimental investigation while the second part is modelling using the response surface methodology (RSM). The experimental investigation was carried out mainly at the concrete and structures laboratory at Universiti Teknologi PETRONAS, Malaysia. The laboratory ambient temperature and humidity were 22 ± 2 degree Celsius and 80±5 %, respectively. The details of fixing position of origami aggregate, casting procedures, testing of mechanical and deformation properties are presented. Furthermore, the procedures for the application of RSM for developing response models and application of multi-objective optimization of variables with multi-criteria settings and subsequent experimental validations of the optimized solution variables are also presented in this chapter. The methodology flowchart is shown in Figure 3.1.

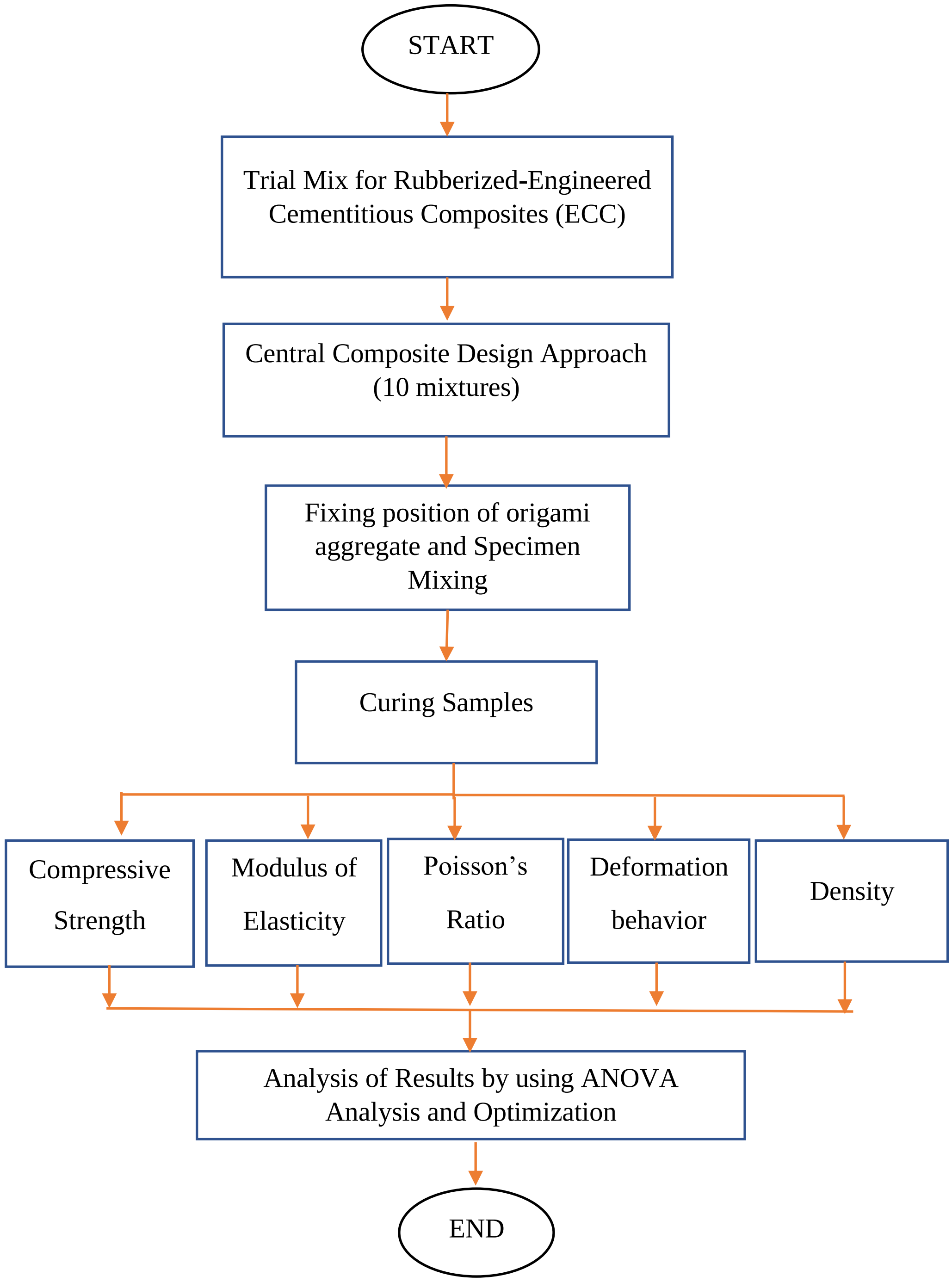

FIGURE 3.1: Project Flowchart

3.2 Materials Used

Rubberized Engineered Cementitious Composites (ECC) will be used in this experiment with fixed position 3D printed origami hollow aggregate in it. The mix proportion for M45-ECC where most researched of ECC have been conducted are used. Table 3.1 shows the materials that are going to be used in this study which consists of the following components:

TABLE 3.1: Materials Used

Materials	Description
3D Printed Origami Hollow Aggregate	Acts as hollow bodies in concrete
Water	Enhance workability of the mix
Ordinary Portland Cement	Essential binding element
Fine Aggregate	Aggregates used are no larger than 4.75mm
Crumb Rubber	As a sand substitute for aggregates
Fly Ash	Used to partially replace cement
Superplasticizer	Additives in high strength concrete
PVA Fibre	Used as Cracks resistance

3.2.1 3D Printed Origami Hollow Aggregate

The origami hollow bodies are inspired by author Pei-Shan Chen. This hollow bodies are made up of polylactic acid, also known as PLA. Polylactic acid is a thermoplastic monomer made from sustainable organic sources like corn starch and sugar cane. PLA has grown in popularity because of its low cost of production from renewable resources. PLA has the world’s second biggest consumption volume of any bioplastic in 2010. The origami hollow bodies are printed by 3D printing lab at Universiti Teknologi PETRONAS. The diameter of the spiky origami hollow bodies is 25mm+/-, max roundness deviation at 0.10 mm, and net filament weight at 350g / 750g. Figure 3.2 shows the picture of the spiky origami hollow bodies.

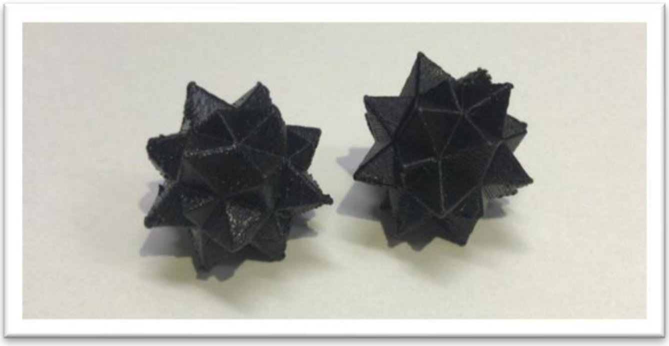

FIGURE 3.2: Picture of Origami Hollow Aggregate

3.2.2 Water

In this experiment, water is a key component mix because it combines all the different components to produce R-ECC. The hydrophilic qualities of the various components are activated by water, which improves flowability, workability, and water tightness. While tap water is fine in this experiment, the pH values of the water must not be too high in acidity or alkalinity because this will cause the R-ECC to lose its qualities. It is critical to use the correct amount of water to ensure that the rubberized concrete produced has the optimal service life.

3.2.3 Ordinary Portland Cement

Ordinary Portland Cement (OPC) Type 1 that met the standards of ASTM C150 (ASTM, 2005f) was used in this experiment. The OPC is one of the most widely used construction materials in the world. OPC is a material manufactured by burning calcareous and argillaceous materials in a big kiln to produce clinker, which is then ground into a fine powder called cement. OPC is a basic component of all types of concrete used in the building industry today, having been discovered in the nineteenth century. The cement's hydrophilic qualities allow it to react well with water, resulting in a waterproof and rigid product. OPC must be handled with extreme caution and kept away from any liquids or humid conditions. Table 3.2 shows the chemical composition and properties of cement.

TABLE 3.2: Chemical Composition and Properties of Cement

Oxide	Cement (%)
CaO	82.10
SiO_2	8.59
Fe_2O_3	3.18
Al_2O_3	2.00
K_2O	0.72
MgO	0.62
SO_3	2.78
P_2O_5	0.46
TiO_2	0.17
MnO	0.15
ZnO	0.03
SrO	0.03
Cuo	0.03
As_2O_3	0.03
ZrO_2	0.03
LOI	2.2
Specific gravity	3.15

3.2.4 Fine Aggregate

Fine aggregates are an important component of any concrete mix design. The type of fine aggregate used in this experiment is ASTM C33 washed river sand from a nearby supplier (ASTM, 2055i). The dimensions of the sand particles are not larger than 4.75 mm (passing) are used. It is critical that the sand is produced in accordance with the specification's standard, and it must be thoroughly dried before use. It is critical to keep in mind that there must be no moisture in the aggregate before mixing, and that sand must not be heavily contaminated by other pollutants.

3.2.5 Crumb Rubber

The crumb rubber preparation process begins with shredding discarded tyres into 100mm-50mm pieces. The granulation process is divided into two stages: the primary stage and the secondary stage, which reduces the rubber particle size to 5mm-0.6mm in size. The primary granulation step separates the steel wire from the tyre chips before the secondary stage takes over. The tyre chips are subsequently ground into smaller mesh sizes, resulting in crumb rubber with the requisite gradation, which is then fed into rolling mills by grinding or cracking.

3.2.6 Fly Ash

All the mixes in the study were made with Class F fly ash (FA) that met the specifications of ASTM C618. FA, as shown in Table 3.1, is classified as class F according to ASTM C618, with a $Si0_2$ + Al_20_3 + Fe_20_3 content of roughly 82.12% and a loss on ignition of less than 6%. (LOI). Due to its availability as a waste from coal-fired power plants, fly ash is one of the cement substitute materials used in concrete materials. The particles of fly ash are spherical in form and range in size from 1 to 100 m.

3.2.7 Superplasticizer (HRWR)

The addition of NS particles to the mixtures resulted in an increase in water demand due to the greater surface area of the NS, which boosts its reactivity. Superplasticizer (HRWR) was employed to alter the mixes to 47 achieve the necessary flowability to keep them self-consolidating. The HRWR utilised is a polycarboxylate ether-based superplasticizer of the third generation. The product by the brand name of Sika ViscoCrete® -2044 was used to attain the desired self-compacting properties at fresh state.

3.2.8 PVA Fibre

The PVA fibres was added to cementitious composites to improve ductility and high strain in cementitious matrix. The volume of the PVA fibre was restricted not to exceed 2% to meet the uniform dispersion, workability, and principles of micromechanics requirements. The PVA fibre manufactured by Kuraray Co. LTD. Japan, coated with oil of 1.2% by fibre weight. The fibre is coated with oil to minimize chemical bonding between the fibre and the cementitious composites.

3.2.9 Materials Quantities and RSM Variable Proportioning

Using the composite design (CCD) option of the RSM, 13 mixes were generated. Three out of five repetitive mixes were removed as there are limited number of origami hollow bodies. Variables considered in the 10 mixes were the Spacing between origami aggregate at 10mm, 15mm, 20mm, and the number of spiky origami hollow aggregate at the range of 9 to 21 (at an interval of 6). The mix proportion for M45-ECC where most researched of ECC have been conducted are used. The cement, Fly-Ash, PVA Fibre, water-binder (W/B) were all kept constants for all the developed mixes as shown in Table 3.3.

TABLE 3.3: RSM Generated Runs and Quantity of Materials

Run	Input Variables		Quantities in Kg/m3						
	A: Spacing between Origami Aggregate (mm)	B: Number of Origami Aggregate	SP	CR	PVA	FA	OPC	Sand	Water
1	15	9	5.78	13	26	705.65	577.35	454	320
2	15	21	5.78	13	26	705.65	577.35	454	320
3	15	15	5.78	13	26	705.65	577.35	454	320
4	10	9	5.78	13	26	705.65	577.35	454	320
5	10	21	5.78	13	26	705.65	577.35	454	320
6	15	15	5.78	13	26	705.65	577.35	454	320
7	20	21	5.78	13	26	705.65	577.35	454	320
8	20	15	5.78	13	26	705.65	577.35	454	320
9	20	9	5.78	13	26	705.65	577.35	454	320
10	10	15	5.78	13	26	705.65	577.35	454	320

3.3 Experimental Procedure

Experimental work from preparation of origami hollow aggregate to testing of mechanical and deformation properties are clearly presented.

3.3.1 Origami Hollow Bodies Aggregate Framing Preparation

This experimental work is carried out by fixing the position origami hollow aggregates. The origami hollow aggregates are held by using thin wires forming a hollow body frame. Different type of frame will be made for the experiment differing from the spacing between origami hollow aggregate and number of origami aggregate used. The spacing between origami aggregate is one of the variables mentioned earlier are 10mm, 15mm and 20mm. Figure 3.3 shows an example of 21 origami aggregate held together by thin wires with 20mm spacing between each origami aggregate. The distance as mentioned between spiky origami hollow aggregate will be the clear distance from neighbouring aggregate. Thirty frames of origami hollow bodies will be made adhering to the 10 mixes developed by the RSM. Three specimens from each mix were prepared. Two specimens from each mix will be used for compressive strength test and 1 for modulus of elasticity test.

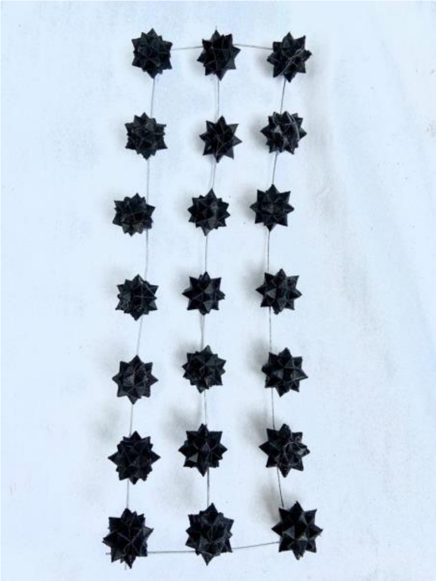

FIGURE 3.3: Picture of Origami Aggregate Held Together by Thin Wires

3.3.2 Mixing and Casting

The materials were prepared based on commonly used M45-ECC mix design. The dry ingredients such as cement, Fly-ash, fine aggregate, and crumb rubber were poured into a double rotation pan type concrete mixer. Concrete mixer was on to mix for two minutes. This was followed by adding water and polycarboxylate-based water reducing admixture. To ensure the PVA fibre to be dispersed and well mix, the PVA fibre was added to the mix gradually form 5 minutes through the mesh opening on top of the pan mixer. This mixer was continued for 5 minutes to achieve a homogenous mix as shown in Figure 3.4. Next, the fresh ECC mix was poured into a 300mm x 150mm cylinder mould for casting. The origami hollow body frame was connected to a thin wire on top to ensure the origami was positioned right in the middle of the cylinder mould. The fresh ECC mix was carefully and gradually poured into the cylinder mould to ensure the origami hollow aggregate stayed in the middle of cylinder mould as shown in Figure 3.5. Three R-ECC samples were made for each mix design. Two will be used for compressive strength test and one for Modulus of elasticity test. Three R-ECC mix without origami hollow bodies were casted for control. After casting, the specimens were placed in water for curing.

FIGURE 3.4: Fresh R-ECC Mix

FIGURE 3.5: Position of Origami Hollow Aggregate during Casting

After 28 days, the concrete has achieved their full strength. Each different type of concrete specimens will be used for the compressive strength test. The concrete specimen's maximum compressive load before failure will be determined. It is then weighted to acquire essential values for determining the density of the concrete specimen before being placed in a compression testing machine to calculate the amount of load required to deform the concrete. Modulus elasticity and Poisson's ratio test will be carried out. Failure pattern of concrete cylinder with origami hollow aggregate will be observed.

3.3.3 Test Procedure for Compressive Strength Test

Specimens were tested for 28 days for their compressive strength. BS EN 206 was adhered in doing compressive strength test [20]. The purpose of this test is to obtain compressive strength of concrete at failure load. The specimen on the lower platen of a 3000 KN compression machine and the bearing block was lowered to slightly bear on the cylinder specimen as shown in Figure 3.6. The compression machine was configured to the cylinder dimension, 300 x 150 mm and the test was commenced. The test was commenced until the cylinder specimen failed. Failure load and stress was recorded.

FIGURE 3.6: Compression Machine and Specimen Before Testing.

3.3.4 Test Procedure for Modulus of Elasticity

For the determination of modulus of elasticity, two samples for each mix were used to determine the average compressive strength. One specimen from each mix proportion was used to determine the modulus of elasticity and Poisson's ration. The specimen was carefully aligned at the centre of the lower platen in the compression testing machine equipped with Compressometer-Extensometer as shown in Figure 3.7. Digital dial gauges on the combined Compressometer-Extensometer in longitudinal and lateral directions were used to measure the deformations. Next, the bearing block was slowly lowered to slightly bear on the specimen. The specimen was loaded to ensure the specimen is seated on the platen and dial gauges respond appropriately. No readings were recorded during this process. The specimens were loaded and the applied load, and longitudinal strain at the point; (1) when the longitudinal strain was at the 50 millionths and (2) when the applied was at 40% of the ultimate loads obtained during compression test. For each specimen, the loading was repeated three times to ensure repeatability of the results. Average readings were taken from the strains obtained from the compression machine and dial gauge, the modulus of elasticity was computed based on the expression in Equation (3.1) as follows.

$$E = \sigma 2 - \sigma 1 / \varepsilon 2 - 0.000050 \qquad (3.1)$$

where:

E = Modulus of elasticity, GPa,

$\sigma 2$ = average stress recorded at 40% of the ultimate load or ultimate stress, MPa

$\sigma 1$ = average stress recorded at longitudinal strain of 0.000050, MPa

$\varepsilon 2$ = average longitudinal strain recorded at 40% of the ultimate load or ultimate stress ($\sigma 2$)

FIGURE 3.7: Compressometer-Extensometer for Modulus of Elasticity Test

3.3.5 Test Procedure for Poisson's Ratio

For the computation and calculation of the Poisson's ratio for the mixtures, the lateral dial gauge was used in accordance with the procedures outlined in ASTM C469 [19]. The recorded loadings and lateral strain obtained at the 50 millionths of the longitudinal strain and 40% of the ultimate load or ultimate stress, respectively. The Poisson's ratios were computed using Equation (3.2) as follows.

$$\mu = (\varepsilon t2 - \varepsilon t1) / (\varepsilon 2 - 0.000050) \qquad (3.2)$$

where:

μ = Poisson's ratio

$\varepsilon t2$ = average transverse strain at 40% of the ultimate load or ultimate stress, $\sigma 2$

$\varepsilon t1$ = average transverse strain recorded at $\sigma 1$,

$\varepsilon 2$ = longitudinal strain equivalent to the stress at $\sigma 2$.

CHAPTER 4

RESULTS AND DISCUSSION

4.1 Results

Test results for density, compressive strength, modulus of elasticity, Poisson's ratio and deformation behaviour of all specimens are clearly presented.

4.1.1 Density

A detailed comparison between density of the 10 mixes to their respective spacing between origami hollow aggregate are demonstrated in Figure 4.1 bar chart form. Table 4.1 shows the density table results obtained from the the 10 mixes labeled M1-M10.

TABLE: 4.1 Density Results

Mix	Spacing between Origami Aggregate (mm)	Number of Origami Aggregate	Density, g/cm^3
Control	NA	NA	1.995
M4	10	9	1.951
M1	15	9	1.924
M9	20	9	1.903
M10	10	15	1.941
M3	15	15	1.909
M6	15	15	1.913
M8	20	15	1.933
M5	10	21	1.886
M2	15	21	1.921
M7	20	21	1.907

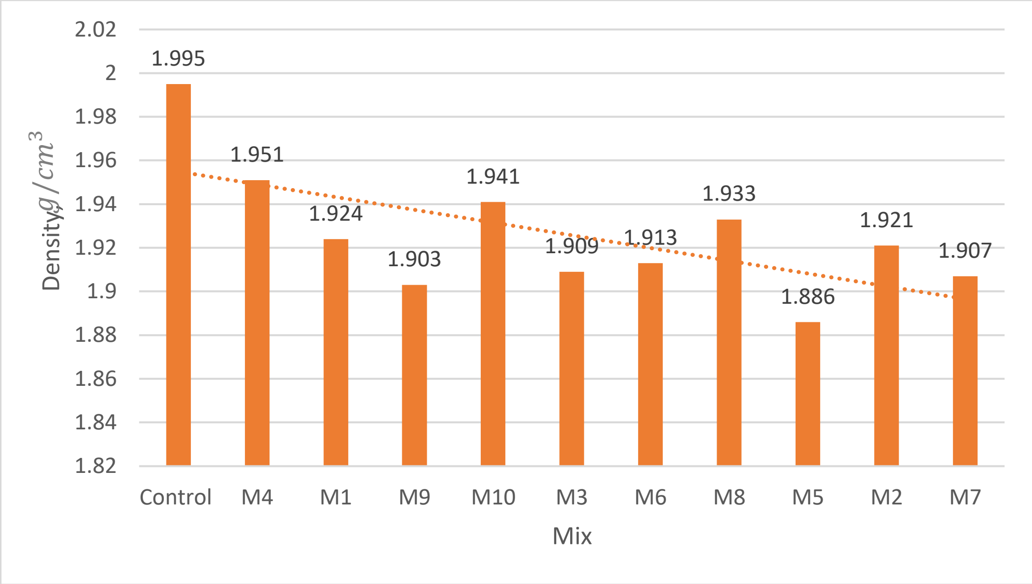

FIGURE 4.1: Density Bar Chart

The overall mix has a average density of 1.918 g/cm^3, while the control mix has density of 1.995 g/cm^3. The results show that the bubble concrete with fixed position origami can reduce its density ranges from 1.886 g/cm^3 – 1.921g/cm^3 . It is about 4% reduced compared to the control mix without the origami hollow bodies. Based on the trend line, it can be seen that as number of origami aggregate increases, the density of bubble concrete decreases. This is due to more origami hollow aggregate creates more hollow cavities, therefore leads to reduction in concrete weight.

The interaction between the spacing between the origami aggregate and the number of origami aggregate was demonstrated with the aid of the 2D contour and 3D response surface plots shown in Figure 4.2 and 4.3 respectively. The graphs are colour coded with the red region presenting the highest density intensity and the blue region representing lowest density intensity respectively. The contour also indicates the variations of the density value over the response surface. Based on observation, the area bounded by the 1.94 contour line and the graph axes at 11 number of aggregate and 12.3 has the highest density intensity. The intensity of density gets reduced as for any combination of the variables below that boundary.

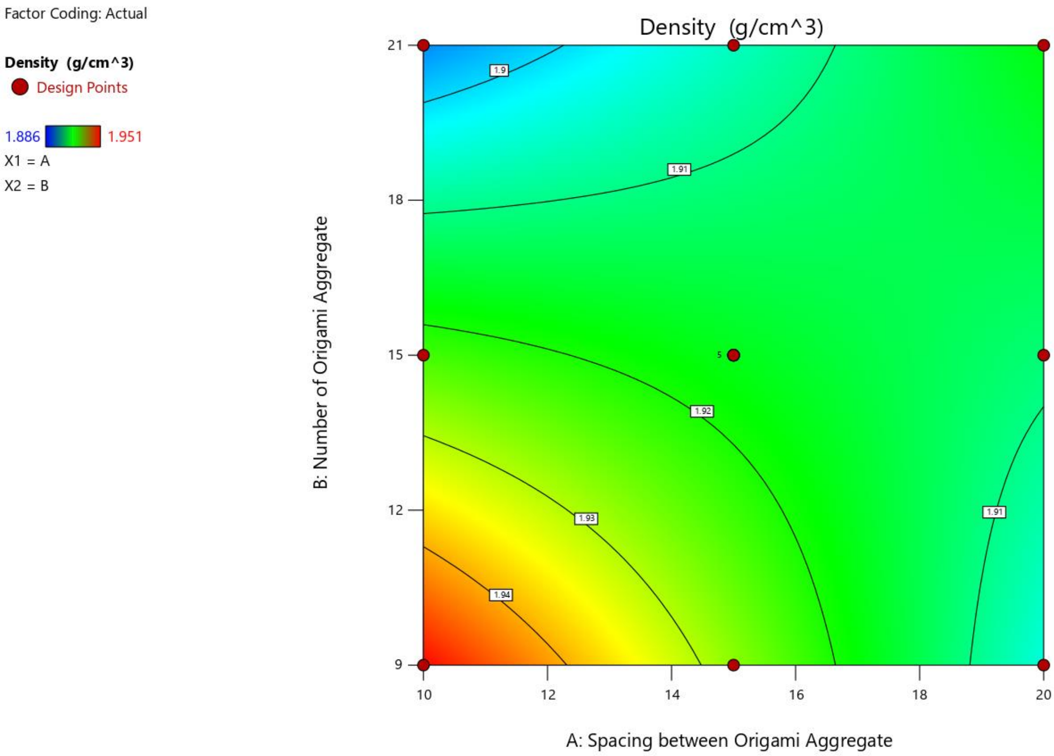

FIGURE 4.2: 2D Contour Graph for Density

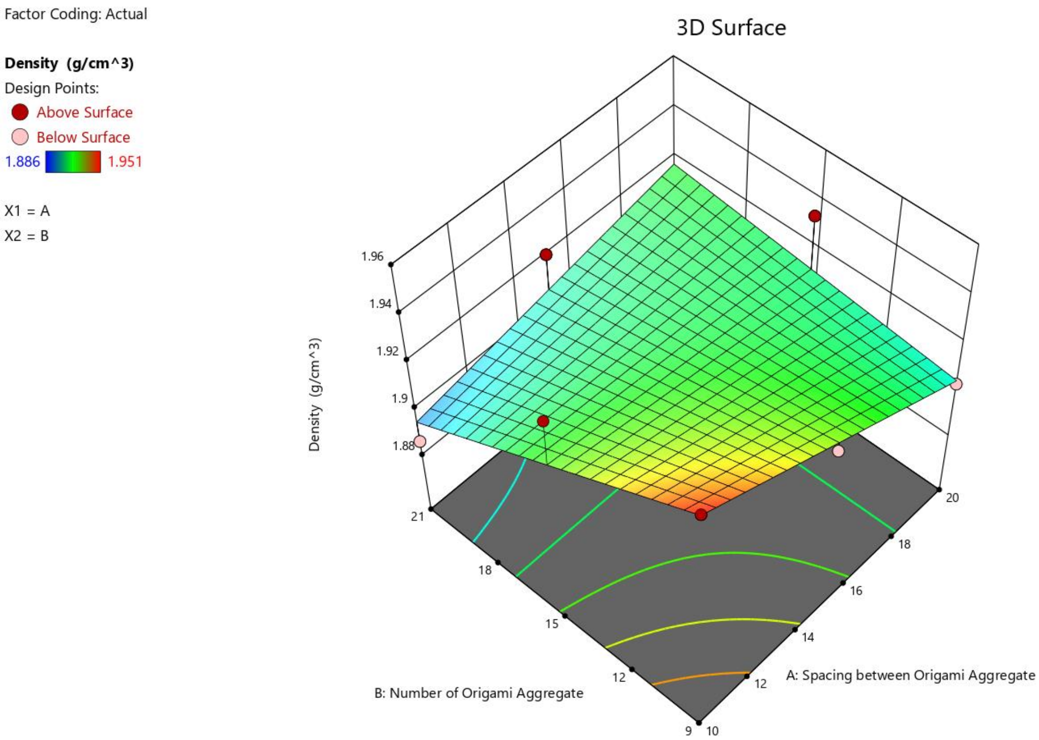

FIGURE 4.3: 3D Response Surface Graph for Density

4.1.2 Compressive Strength

A detailed comparison between compressive strength of the 10 mixes to their respective spacing between origami hollow aggregate are demonstrated in Figure 4.4 bar chart form. Table 4.2 shows the table results obtained from the 28 day strength of the 10 mixes labeled M1-M10.

TABLE 4.2: 28 days Compressive Strength Test Results

Mix	Spacing between Origami Aggregate (mm)	Number of Origami Aggregate	28-Days Compressive Strength (MPa)
M4	10	9	33.69
M10	10	15	23.41
M5	10	21	18.58
M1	15	9	30.58
M3	15	15	28.9
M6	15	15	19
M2	15	21	30.63
M9	20	9	31.49
M8	20	15	34.97
M7	20	21	28.97

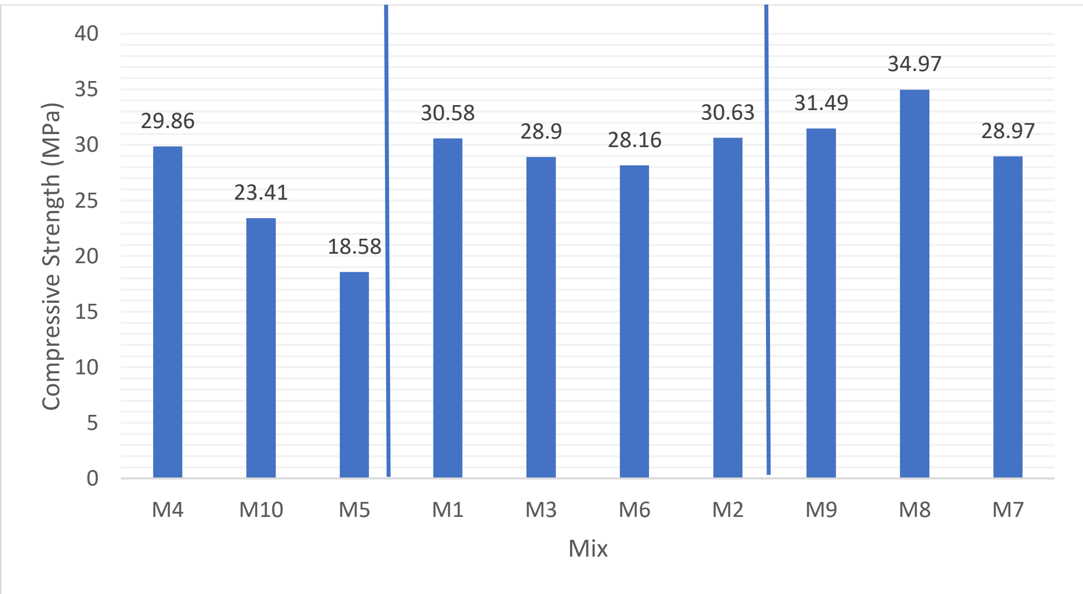

FIGURE 4.4: Compressive Strength Bar Chart

The highest 28 days strength belongs to Mix 8 which has 15 number of origami hollow bodies with 20mm spacing between origami aggregates. The lowest 28-days compressive strength belongs to Mix 5 which has 21 number of origami hollow aggregate with 10mm spacing between origami aggregates. As for spacing of 10mm, Mix 4 consists of 9 origami hollow agregate having a compressive strength of 29.86 MPa while Mix 5 consists of 21 origami hollow aggregate is 18.58 MPa. This shows that higher number of hollow bodies exhibits lower compressive strength. From each particular spacing from the figure 4.4 bar chart above, a decreasing trend in compressive strength is observed. It can be said that the higher the number of origami aggregate, the lower the compressive strength. The average compressive strength of control Rubberized ECC was 34.56 MPa, while the average strength of the Rubberized ECC with fixed position origami model is 28.55 MPa.

The origami model can suppress the hollow bodies to generate vertical compression and lateral expansion at the same time, so that the stress in the concrete is evenly distributed. The cross-sectional area of origami hollow body model is smaller than the sphere and cubic concave model from previous research, it needs to carry greater stress and concrete will break earlier [10]. Consequently, the strength performance of RECC with this origami hollow aggregate is lower than the conventional control concrete.

The failure mode of R-ECC containing origami hollow aggregate is presented in Figure 4.5 below. According to the observation and results obtained, the R-ECC with origami hollow aggregate possess high ductility as it does not strip or break when it is subjected to load. It is not brittle as the R-ECC do not strip off even when failure load has achieved. The R-ECC cracks diagonally at an angle of roughly 45 degrees, which can be said it might be the surface of hollow aggregate that affect the adhesion between the R-ECC. Some specimen produces not much cracks as PVA fibre acts as crack resistance in the R-ECC and crumb rubber boost the ductility of the Rubberized ECC.

FIGURE 4.5: Failure Mode of Specimen

Figure 4.6 shows compressive strength from respective group of number of origami hollow bodies. A trend can be seen that as spacing between origami hollow aggregate increases, the compressive strength increases. At group with number of origami aggregate of 15, Mix 10 consists 10mm spacing has a compressive strength of 23.41 MPa while Mix 8 consists of 20mm spacing has a compressive strength of 34.97 MPa. The mixes having higher spacing exhibits higher compressive strength. This is due to shorter distance between hollow bodies will affect each other more when load is subjected.

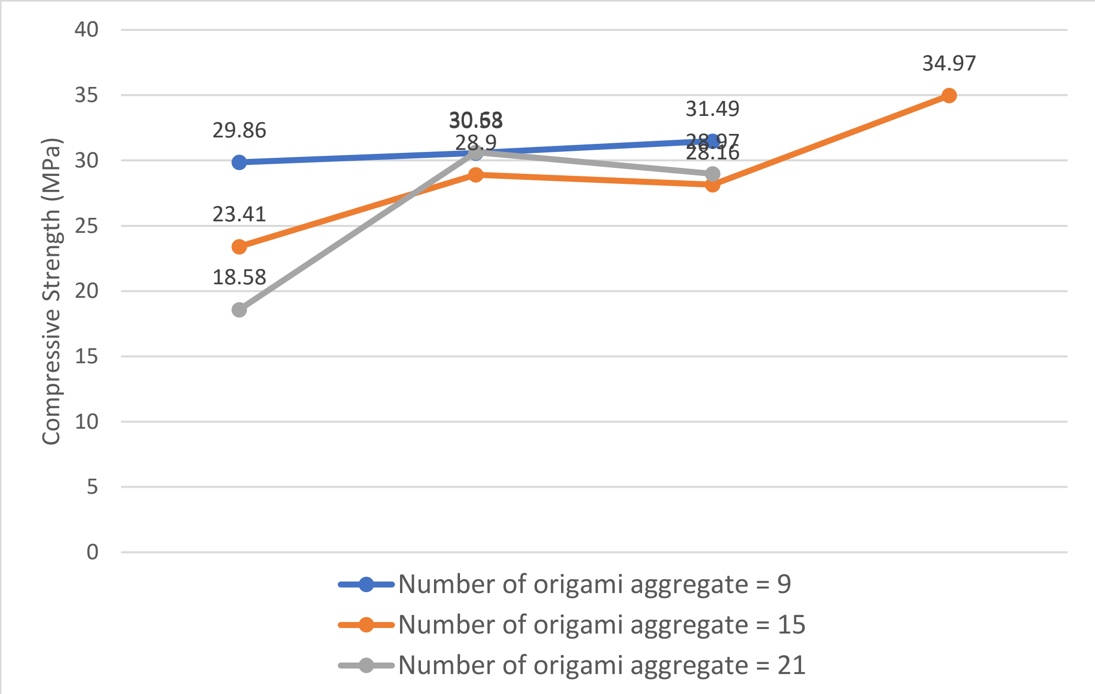

FIGURE 4.6: Compressive at Each Group of Number of Origami Aggregate

The 2D and 3D response surface plots showed in Figure 4.7 and Figure 4.8 respectively indicate the influence of the factor and their interaction on compressive strength. The red zone indicates regions of higher compressive strength while the blue regions indicate low compressive strength value. Based on observation, the area bounded by the 32MPa contour line and the graph axes at 18 mm spacing has the highest compressive strength intensity. The intensity of compressive strength gets reduced as the increment of origami aggregate.

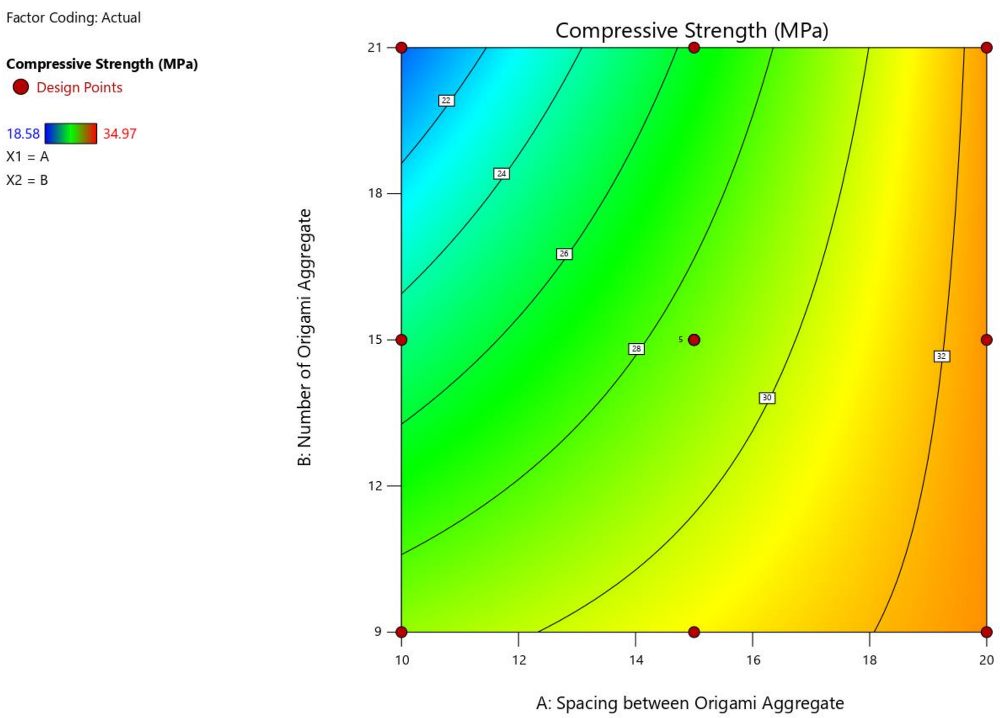

FIGURE 4.7: 2D Response Surface Contour Graph for Compressive Strength

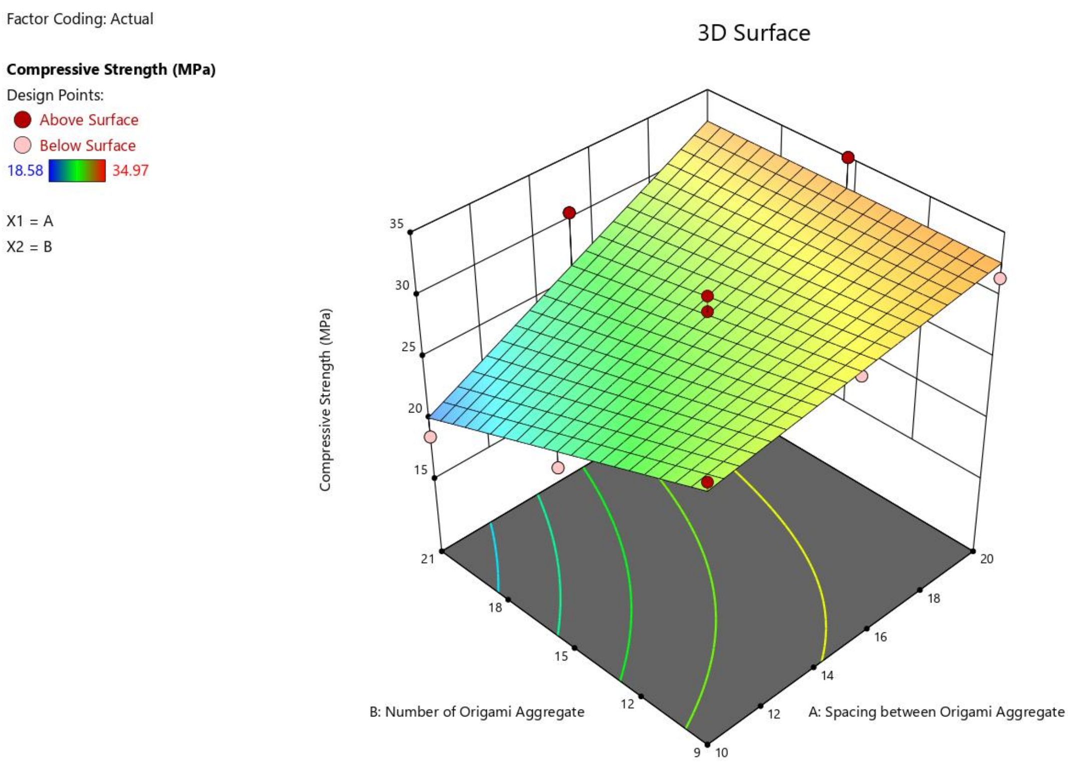

FIGURE 4.8: 3D Response Surface Graph for Compressive Strength

4.1.3 Modulus of Elasticity

Results are calculated from the formula mentioned previous chapter. A detailed comparison between modulus of elasticity of the 10 mixes to their respective spacing between origami hollow aggregate are demonstrated in Figure 4.9 in bar chart form. Table 4.3 shows the modulus of elasticity table results obtained of the 10 mixes labeled M1-M10.

TABLE 4.3: Modulus of Elasticity Test Results

Mix	Spacing between Origami Aggregate (mm)	Number of Origami Aggregate	Modulus of Elasticity (GPa)
M4	10	9	17.57
M10	10	15	9.53
M5	10	21	9.52
M1	15	9	14.28
M3	15	15	13.09
M6	15	15	11.3
M2	15	21	13.67
M9	20	9	15.8
M8	20	15	19.73
M7	20	21	18.69

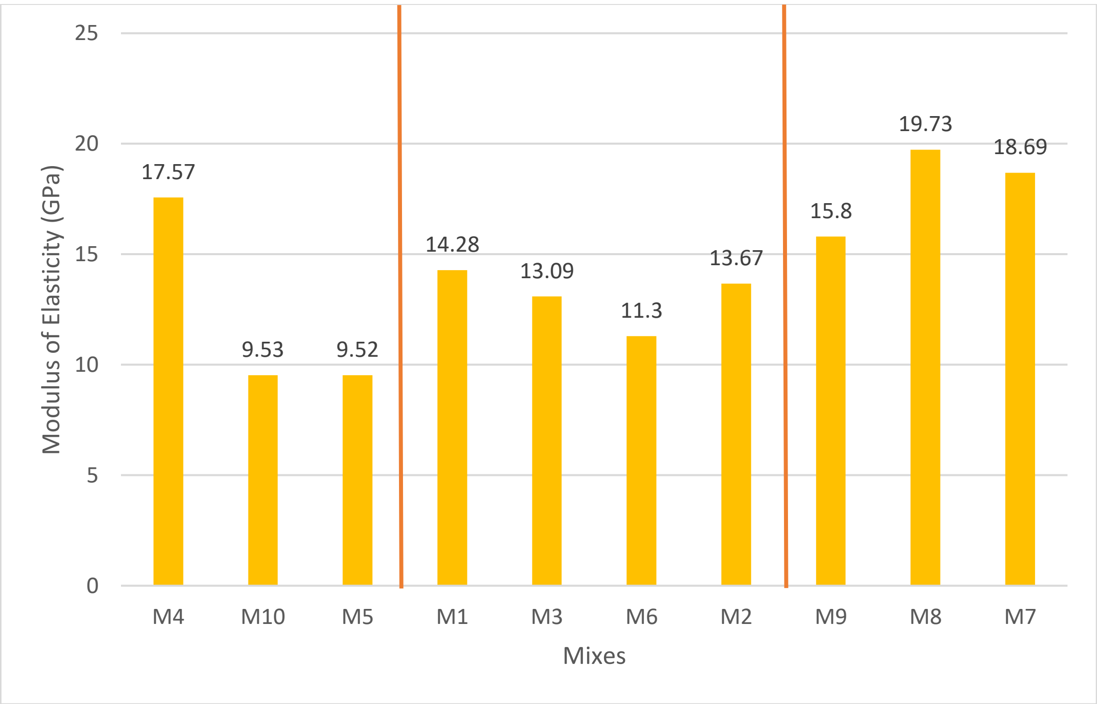

FIGURE 4.9: Modulus of Elasticity Bar Chart Results

The mix with the highest modulus of elasticity which is 19.73 GPa belongs to Mix 8 which has 15 number of origami hollow bodies with 20mm spacing between origami aggregates. The mix with the lowest modulus of elasticity which is 9.52 GPa belongs to Mix 5 which has 21 number of origami hollow aggregate with 10mm spacing between origami aggregates. As for spacing of 10mm, Mix 4 consists of 9 origami hollow agregate having a modulus of elasticity of 17.57 GPa while Mix 5 consists of 21 origami hollow aggregate is 9.52 GPa. This shows that higher number of hollow bodies exhibits lower modulus of elasticity. From each particular spacing from the figure 4.7 bar chart above, a decreasing trend in modulus of elasticity as increase in number of origami hollow aggregate is observed. It can be said that the higher the number of origami aggregate, the lower the compressive strength. This is due to when the number of origami aggregate is high, the concrete exhibits lower deformation capacity therefore the Rubberized ECC becomes more deformable. Consequently, the lower the modulus of elasticity. The 10mm and 15 mm spacing shows the consistent decrement of elastic moduluscity while for 20mm the value is inconsistent as M8 mix surpasses the M7 mix. The modulus of elasticity of control Rubberized ECC was 18.73 GPa, while the average modulus of elasticity of the Rubberized ECC with fixed position origami model is 14.31 GPa. As for the spacing it can be seen that the higher the spacing between origami hollow aggregate, the higher the modulus of elasticity. The shorter the distance between each aggregate creates more interation between the aggregate. The stress aggregate experience among themselves could affect the overall strength of the Rubberized ECC.

The interation between the number of origami aggregate and spacing between origami hollow aggregate was presented with the aid of a 2D contour and 3D response surface plot as shown in Figure 4.10 and Figure 4.11 respectively. The red zones indicate region with high intensity of modulus of elasticity. The interation of the independent variable is visually expressed by the colour coded diagrams. The area bounded by 18 number of origami aggregate and spacing represent the highest modulus of elasticity region. Any area beyond this boundary will lead to lower value of modulus of elasticity that may not be desirable.

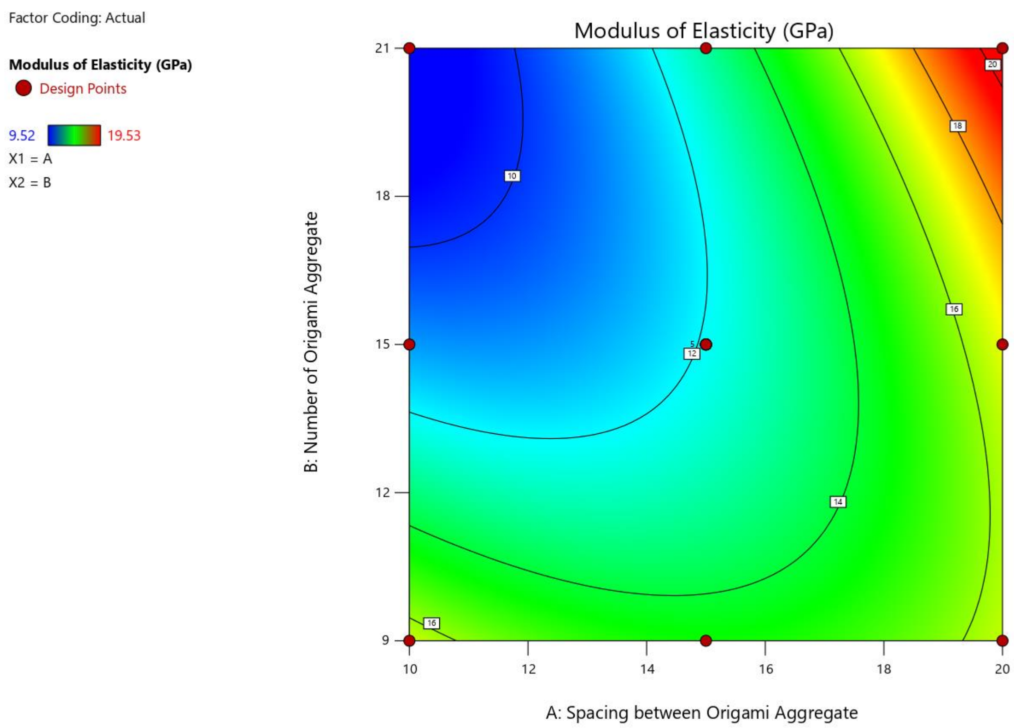

FIGURE 4.10: 2D Response Surface Contour Graph for Modulus of Elasticity

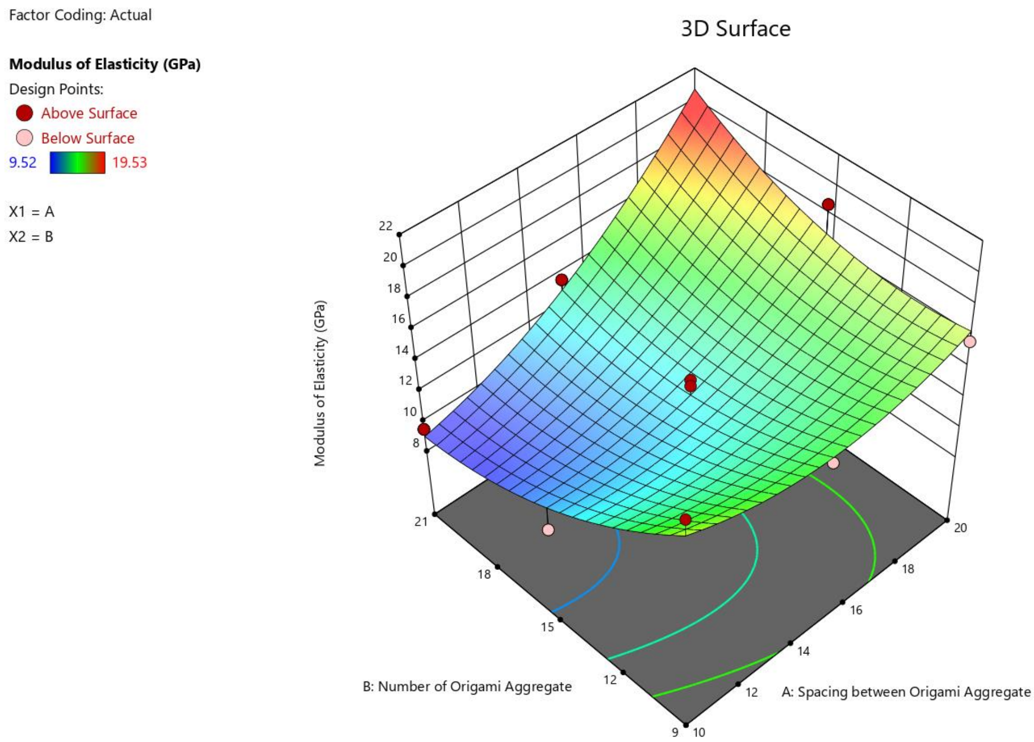

FIGURE 4.11: 3D Response Surface Graph for Modulus of Elasticity

4.1.4 Poisson's Ratio

Results are calculated from the formula mentioned previous chapter. A detailed comparison between modulus of elasticity of the 10 mixes to their respective spacing between origami hollow aggregate are demonstrated in Figure 4.12 in bar chart form. Table 4.4 shows the Poisson's ratio results obtained of the 10 mixes labeled M1-M10.

TABLE 4.4: Poisson's Ratio results

Mix	Spacing between Origami Aggregate (mm)	Number of Origami Aggregate	Poisson's Ratio
M4	10	9	0.174
M10	10	15	0.635
M5	10	21	0.579
M1	15	9	0.395
M3	15	15	0.692
M6	15	15	0.707
M2	15	21	0.556
M9	20	9	0.317
M8	20	15	0.091
M7	20	21	0.286

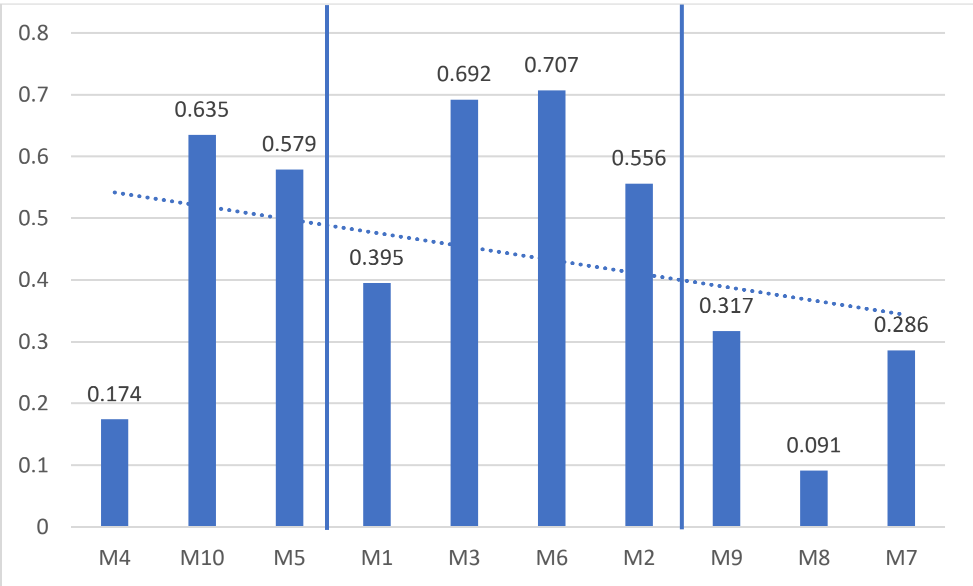

FIGURE 4.12: Poisson's Ratio Results Graph

The mix with the highest Poisson's ratio which is 0.707 belongs to Mix 6 which has 15 number of origami hollow bodies with 15 mm spacing between origami aggregates.

The mix with the Poisson's ratio which is 0.091 belongs to Mix 8 which has 15 number of origami hollow aggregate with 20 mm spacing between origami aggregates. Certain Poisson's ratio results obtained are not complying to the Poisson's ratio range that is due to human error when conducting experiment. Based on observation of the trend line, it is noted that the Poisson's ratio of the mix increases with the increase number of origami hollow aggregate. This shows that higher number of hollow bodies exhibits higher Poisson's ratio. The origami hollow aggregate possesses a much deformation capability, when the ECC subjected to stress, its deformation resistance is considerably lesser, causing the ECC to experience a larger axial compression.

The interation between the number of origami aggregate and spacing between origami hollow aggregate was presented with the aid of a 2D contour and 3D response surface plot as shown in Figure 4.13 and Figure 4.14 respectively. The red zones indicate region with high intensity of Poisson's ratio. The interation of the independent variable is visually expressed by the colour coded diagrams. The area bounded red visualize the number of origami aggregate exibits high Poisson's ratio.

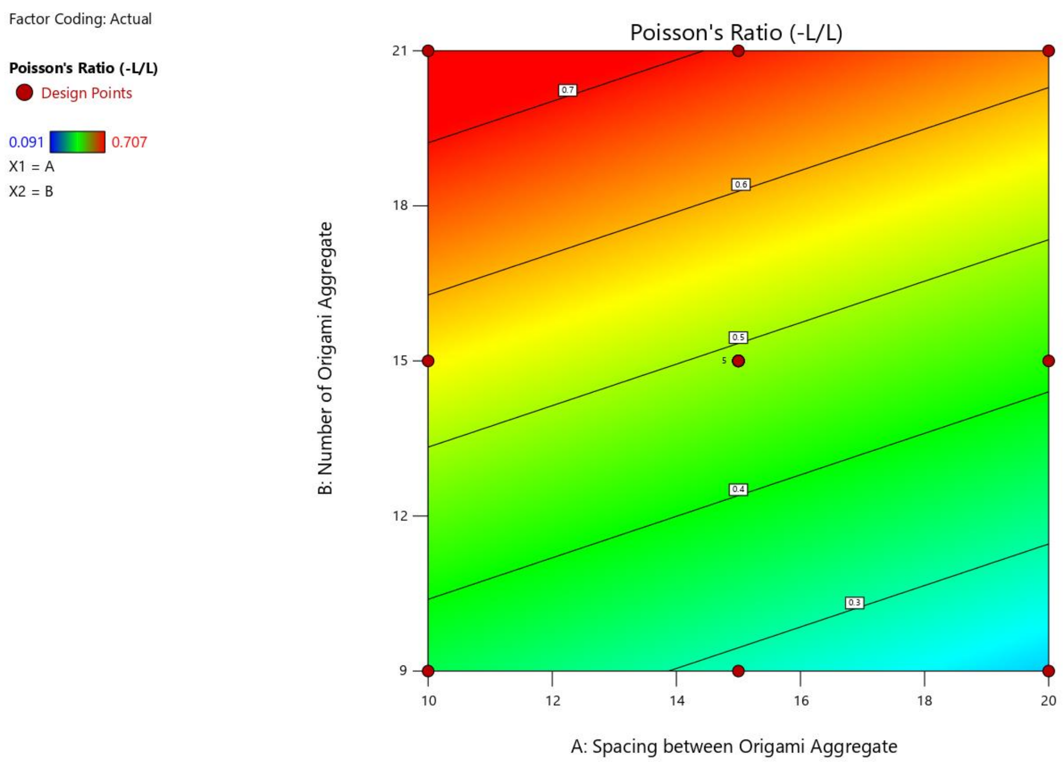

FIGURE 4.13: 2D Response Surface Contour Graph for Poisson's Ratio

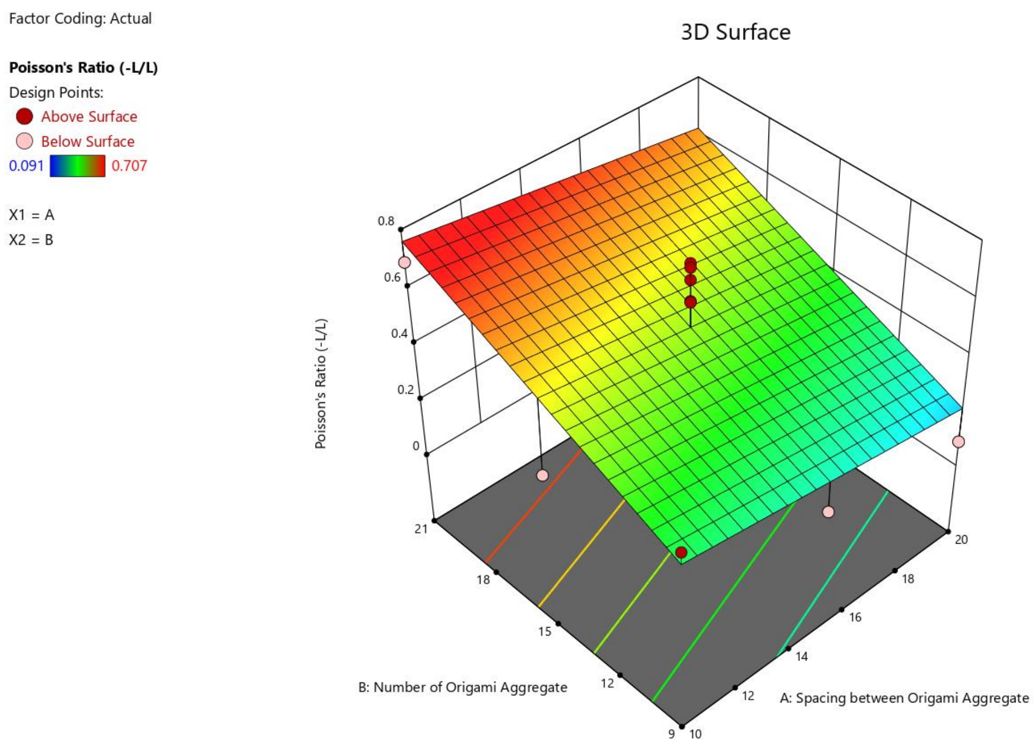

FIGURE 4.14: 3D Response Surface Surface Plot for Poisson's Ratio

4.2 RSM Modelling and ANOVA Analysis

These equations were developed to be accurate in predicting model responses at various levels of each factor. The levels for each factor should be defined in 42 their original units, and the equation should not be used to calculate the relative impact of each factor because the coefficients are scaled to fit the units of each factor, and the intercept is not in the centre of the design space. The model equation (in coded terms) developed for three responses are presented in Equations 4.1 to 4.4.

$$D = 1.92 - 0.0058 * A - 0.0107 * B + 0.01725 * AB \quad (4.1)$$

$$CS = 28.64 + 3.93 * A - 2.29167 * B + 2.19 * AB \quad (4.2)$$

$$ME = 12.08 + 2.9 * A - 0.821667 * B + 2.945 * AB + 1.87 * A^2 + 1.735 * B^2 \quad (4.3)$$

$$PR = 0.4885 - 0.0682 * A + 0.2038 B \quad (4.4)$$

The ANOVA analysis was performed at 95% confidence interval corresponding to 5% level of significance. Table 4.1 shows the ANOVA summary for all the responses. With the analysis performed at a p-value of 0.05, all model terms with p-value >F less than 0.05 is significant. Hence the developed models were all significant with p-values of 0.0378, 0.0038, 0.0017 and 0.0259 for density, compressive strength, modulus of elasticity and Poisson's ratio respectively. Similarly, for the density and compressive strength, modulus of elasticity and Poisson's ratio are significant model terms. For A, B, AB and B^2 are the significant model terms. Additionally, for the model to fit, the lack of fit P-value > F must be insignificant. In this case, all the models exhibited an significant value of the lack of fit except for the modulus of elasticity. This indicates the adequacy of the models for predicting the responses.

TABLE 4.1: ANOVA Summary

Response	**Source**	**Sum of Squares**	**Df**	**Mean Square**	**F-value**	**P-value**	**Significance**
Density	Model	0.0021	3	0.0007	4.33	0.0378	Yes
	A-Spacing	0.0002	1	0.0002	1.28	0.2875	No
	B- NA	0.0007	1	0.0007	4.27	0.0687	Yes
	AB	0.0012	1	0.0012	7.45	0.0232	Yes
	Residual	0.0014	9	0.0002			
	Lack of Fit	0.0014	5	0.0003	89.06	0.0003	Yes
	Pure Error	0	4	3.20E-06			
Compressive Strength	Model	143.36	3	47.79	9.45	0.0038	Yes
	A-Spacing	92.67	1	92.67	18.33	0.002	Yes
	B- NA	31.51	1	31.51	6.23	0.0341	Yes
	AB	19.18	1	19.18	3.79	0.0833	No
	Residual	45.51	9	5.06			
	Lack of Fit	42.78	5	8.56	12.53	0.0148	Yes
	Pure Error	2.73	4	0.6829			
Modulus of Elasticity	Model	118.21	5	23.64	13.7	0.0017	Yes
	A-Spacing	50.46	1	50.46	29.24	0.001	Yes
	B- NA	4.05	1	4.05	2.35	0.1693	No
	AB	34.69	1	34.69	20.1	0.0029	Yes
	A^2	9.66	1	9.66	5.6	0.0499	Yes
	B^2	8.31	1	8.31	4.82	0.0642	No
	Residual	12.08	7	1.73			
	Lack of Fit	9.42	3	3.14	4.72	0.0841	No
	Pure Error	2.66	4	0.6657			
Poisson's Ratio	Model	0.2772	2	0.1386	5.38	0.0259	Yes
	A-Spacing	0.0279	1	0.0279	1.08	0.3227	No
	B- NA	0.2493	1	0.2493	9.68	0.011	Yes
	Residual	0.2576	10	0.0258			
	Lack of Fit	0.2423	6	0.0404	10.59	0.0194	Yes
	Pure Error	0.0153	4	0.0038			

Another measure for the strength of a model is the coefficient of determination (R2). The R2 is measure of how close the data is to the fitted model. The higher the R2 value, (on a scale of 0 to 100%) the better the model fits the data. In the case of the developed models in this research, the R^2 values are 59%, 75%, 90% and 51% for density and compressive strength, modulus of elasticity and Poisson's ratio respectively as presented in Table 4.5. These high values of the coefficient of determination indicate how well the models fit the data. In the same vein, the difference between Adjusted R^2 and predicted R^2 should be less than 0.2 for the model to fit. In this case, the difference between these parameters for some models are less than 0.2 as can be seen from Table 4.2 but some are not complying to it. Similarly, the adequate precision value (Adeq. Precision) measures the signal to noise ratio, and a value of more than 4 is desirable. In the case of the developed models, the Adeq. Precision values are 7.9634, 9.9759, 13.0991, and 7.056 for density, compressive strength, modulus of elasticity and Poisson's ratio respectively. These values shows that there is a good signal, and the models can be used to navigate the design space.

TABLE 4.2: Model Validation Parameters

Model Validation Parameters	**Responses**			
	Density	**Compressive Strength (MPa)**	**Modulus of Elasticity (GPa)**	**Poisson's Ratio**
Std. Dev.	0.0126	2.25	1.31	0.1605
Mean	1.92	28.64	13.74	0.4885
C.V. %	0.6594	7.85	9.56	32.86
R^2	0.5909	0.7591	0.9073	0.5183
Adjusted R^2	0.4546	0.6787	0.8411	0.422
Predicted R^2	-0.0648	-0.0267	0.2381	0.2425
Adeq Precision	7.9634	9.9759	13.0991	7.056
PRESS	0.0037	193.92	99.26	0.4051
-2 Log Likelihood	-81.53	53.18	35.94	-14.09
BIC	-71.27	63.44	51.33	-6.39
AICc	-68.53	66.18	61.94	-5.42

Two of the most popular model diagnostic tools are the Normal plots of Residuals and the Actual versus Predicted graphs. As shown in Figures 4.15 to 4.18, the nature of the data points distribution around the lines of fit suggests the adequacy of the models.

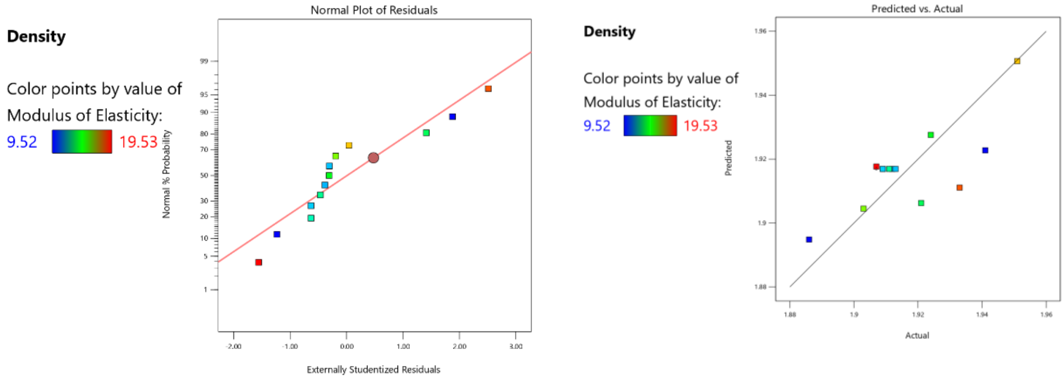

FIGURE 4.15: Model Diagnostic Plots for density (a) Normal Plot of Residuals (b) Predicted versus Actual Plot

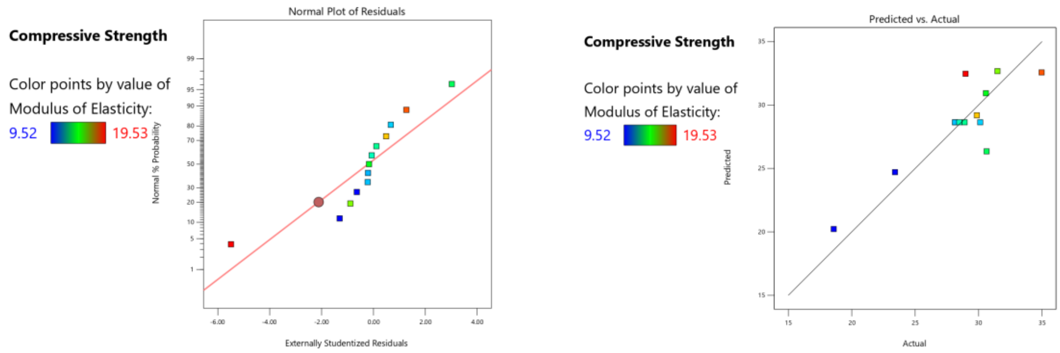

FIGURE 4.16: Model Diagnostic Plots for CS (a) Normal Plot of Residuals (b) Predicted versus Actual Plot

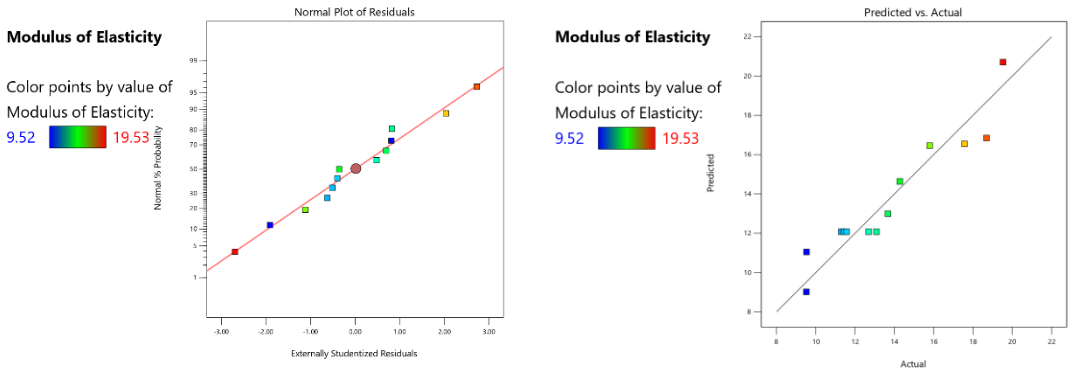

FIGURE 4.17: Model Diagnostic Plots for ME (a) Normal Plot of Residuals (b) Predicted versus Actual Plot

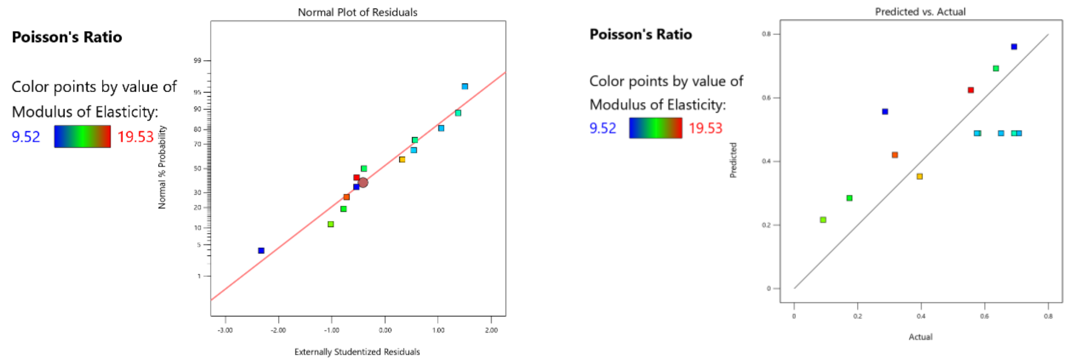

FIGURE 4.18: Model Diagnostic Plots for PR (a) Normal Plot of Residuals (b) Predicted versus Actual Plot

4.3 Optimization

An optimum spacing between origami aggregate and number of origami hollow aggregate that will give the best mechanical and deformation properties of the Rubberized ECC were identified. Optimization was carried out as part of the RSM Analysis. This is achieved by setting objectives for the variables which are the input factors with various criteria to attain the objective function. The optimization outcome is accessed by the desirability value, which ranges from 0 to 1.

The value of desirability in this experiment obtained is 0.835 which is desirable. It is high considering the nature factor affecting the experiment. The optimum values of the input factors generated by the optimization are 20 and 9 for spacing between origami hollow aggregate and number of origami hollow aggregate respectively. These values are presumed by the system to yield an optimum mechanical properties value of 1.904 g/cm^3, 32.67 MPa, 16.46GPa and 0.21 for density, compressive strength, modulus of elasticity and Poisson's ratio respectively. The optimization solution and the desirability value are presented in Figure 4.19 and Figure 4.20 as ramps and 3D-response surface diagram respectively.

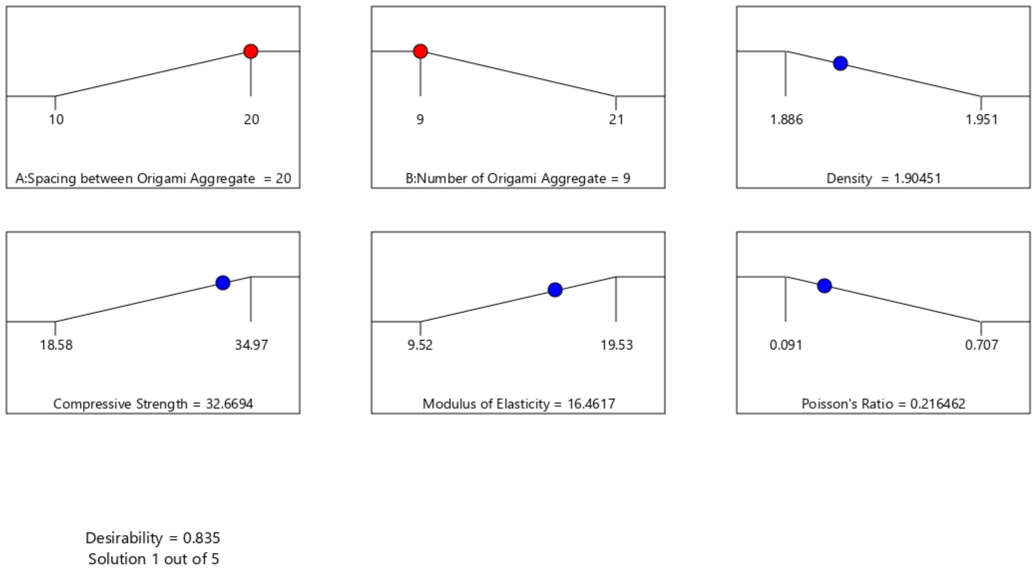

FIGURE 4.19: Optimization Ramp

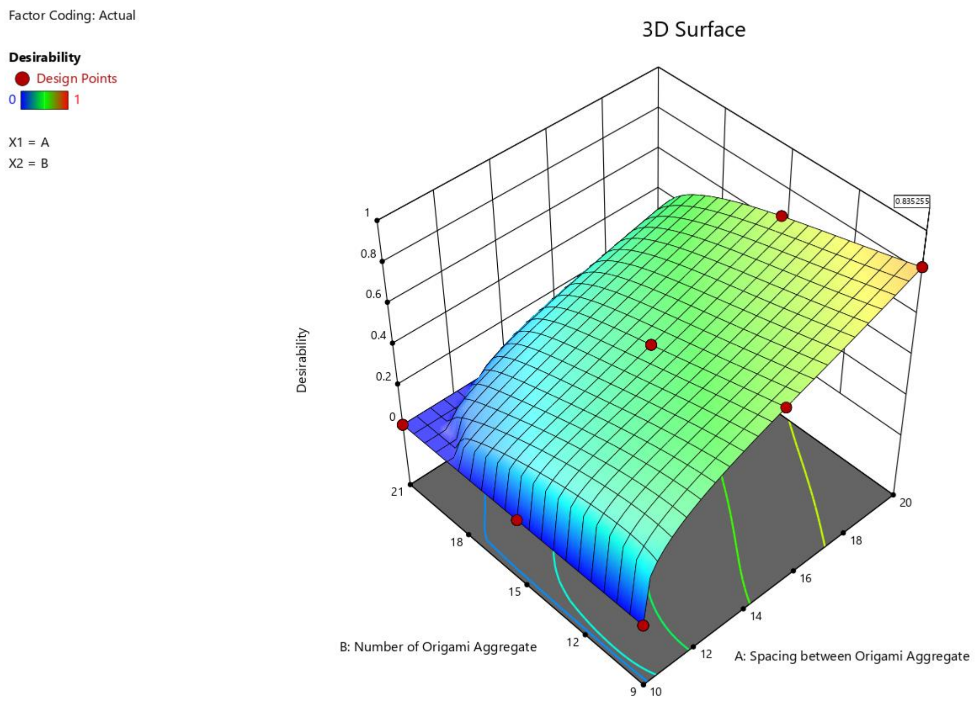

FIGURE 4.20: 3D response Surface Diagram for Desirability

CHAPTER 5

CONCLUSION AND RECOMMENDATION

5.1 Conclusion

At the end of this research, the following conclusions are drawn

1. Rubberized Engineered Cementitious Composites (ECC) containing 3D-Printed origami hollow aggregate can reduce its density to 1.886 g/cm^3 – 1.921 g/cm^3 (94.5%-96.2%, compared to control Rubberized ECC), its average compressive strength reaches 28.55 MPa, Modulus of Elasticity and Poisson's ratio of 14.31 GPa and 0.21 respectively. It has a 4% reduction in density compared to control mix. The higher number of origami hollow hollow bodies exhibits lower strength. Mechanical and deformation properties of the Rubberized ECC were negatively affected by the increased number of origami hollow bodies.
2. Rubberized ECC mixes were developed by using response surface methodology (RSM) with spacing between origami hollow aggregate and number of origami aggregate as the input factor while density, compressive strength, modulus of elasticity and Poisson's ratio as the responses. Optimization was carried out which has the desirability value of 0.835. Nine number of origami hollow bodies with 20 mm spacing are found to yield optimum mechanical and deformation properties.

5.2 Recommendation

1. In order to obtain a more significant reduction in density, more hollow bodies in concrete should be used and utilized.
2. Further research should be conducted on tensile strength, durability behaviour and shrinkage analysis.
3. Finite Element Analysis can be carried out to study the stress distribution and failure mechanism of origami hollow aggregate inside the concrete.

References

1. Haque, M., Al-Khaiat, H., & Kayali, O. (2004). Strength and durability of lightweight concrete. *Cement and Concrete Composites*, *26*(4), 307–314. https://doi.org/10.1016/s0958-9465(02)00141-5
2. Min, H.Z.; Odd, E.G. Mechanical Properties of High-Strength Lightweight Concrete. Mater. J. 1991, 88, 240–247.
3. Kan, A., & Demirboğa, R. (2009). A novel material for lightweight concrete production. *Cement and Concrete Composites*, *31*(7), 489–495. https://doi.org/10.1016/j.cemconcomp.2009.05.002
4. Lo, T. Y., Tang, W., & Cui, H. (2007). The effects of aggregate properties on lightweight concrete. *Building and Environment*, *42*(8), 3025–3029. https://doi.org/10.1016/j.buildenv.2005.06.031
5. Palle, N.-C.; Tommy, P.H.N. Modal determination of the effect of bond between coarse aggregate and mortar on the compressive strength of concrete. J. Proc. 1969, 66, 66–67.
6. Abdullah, M. M. A. B., Hussin, K., Bnhussain, M., Ismail, K. N., Yahya, Z., & Abdul Razak, R. (2012). Fly Ash-based Geopolymer Lightweight Concrete Using Foaming Agent. *International Journal of Molecular Sciences*, *13*(6), 7186–7198. https://doi.org/10.3390/ijms13067186
7. Fahrizal, Z.; Mahyuddin, R. Performance and characteristic foamed concrete mix design with silica fume for housing development. Int. J. Acad. Res. 2011, 3, 1198–1206.
8. Ducman, V., & Mirtič, B. (2009). The applicability of different waste materials for the production of lightweight aggregates. *Waste Management*, *29*(8), 2361–2368. https://doi.org/10.1016/j.wasman.2009.02.013

9. Chen, P.-S. A study report on light weight concrete mixed with high strength hollow bubbles. In Proceeding of AIJ Tohoku Chapter Architectural Research Meeting (Kouzoukei); Architectural Institute of Japan: Tokyo, Japan, 2008; No.71; pp. 57–62.
10. Chen, P.-S. Bubble Concrete. Japan Patent Office JP2008308395, 25 December 2008. Available online: https://patentfield.com/ patents/JP2007181500A (accessed on 25 December 2008).
11. Lim, T. J., Smith, B., & McDowell, D. (2002). Behavior of a random hollow sphere metal foam. *Acta Materialia*, *50*(11), 2867–2879. https://doi.org/10.1016/s1359-6454(02)00111-8
12. Schnellenbach-Held, M., & Pfeffer, K. (2002). Punching behavior of biaxial hollow slabs. *Cement and Concrete Composites*, *24*(6), 551–556. https://doi.org/10.1016/s0958-9465(01)00071-3
13. S. Wang, (2005). "Micromechanics based matrix design for engineered cementitious composites,"
14. V. C. Li, (2008). "Engineered Cementitious Composites (ECC) Material, Structural, and Durability Performance,"
15. L.-L. Kan, H.-S. Shi, A. R. Sakulich, and V. C. Li, (2010). "Self-Healing Characterization of Engineered Cementitious Composite Materials," ACI Materials journal, vol. 107, no. 6.
16. V. C. Li, (2002). "Advances in ECC research," ACI Special Publications, vol. 206, pp. 373-400.
17. J. R. Homrich and A. E. Naaman, "Stress-strain properties of SIFCON in compression," Special Publication, vol. 105, pp. 283-304, 1987.
18. M. Wu, B. Johannesson, and M. Geiker, (2012). "A review: Self-healing in cementitious materials and engineered cementitious composite as a self-

healing material," Construction and Building Materials, vol. 28, no. 1, pp. 571-583, 2012/03/01/.

19. G. Yıldırım, Ö. K. Keskin, S. B. Keskin, M. Şahmaran, and M. Lachemi, (2015) "A review of intrinsic self-healing capability of engineered cementitious composites: Recovery of transport and mechanical properties," Construction and Building Materials, vol. 101, no. Part 1, pp. 10-21, 2015/12/30
20. F. Aslani, J. Kelin, (2018) Assessment and development of high-performance fibre-reinforced lightweight self-compacting concrete including recycled crumb rubber aggregates exposed to elevated temperatures, J. Clean. Prod. 200: 1009–1025.
21. Z. Zhang, H. Ma, S. Qian. (2015). Investigation on properties of ECC incorporating crumb rubber of different sizes, J. Adv. Concr. Technol. 13 (5): 241–251.
22. Yan, X.; Chen, P.-S.; Al-Fakih, A.; Liu, B.; Mohammed, B.S.; Jin, J. Experiments and Mechanical Simulation on Bubble Concrete: Studies on the Effects of Shape and Position of Hollow Bodies Mixed in Concrete. Crystals 2021, 11, 858. https://doi.org/10.3390/ cryst11080858
23. D. Montgomery, (2005). "Design and Analysis of Experiments, Six Edition, John Wiley&Sons," ed: Inc,
24. F. Bayramov, C. Taşdemir, and M. Taşdemir, (2004). "Optimisation of steel fibre reinforced concretes by means of statistical response surface method," Cement and Concrete Composites, vol. 26, no. 6, pp. 665-675.
25. M. A. Bezerra, R. E. Santelli, E. P. Oliveira, L. S. Villar, and L. A. Escaleira, (2008). "Response surface methodology (RSM) as a tool for optimization in analytical chemistry," Talanta, vol. 76, no. 5, pp. 965-977.

26. T. E. Murphy, K.-L. Tsui, and J. K. Allen, (2005) "A review of robust design methods for multiple responses," Research in Engineering Design, vol. 15, no. 4, pp. 201-215.

27. H. Savastano, S. Santos, M. Radonjic, and W. Soboyejo, (2009). "Fracture and fatigue of natural fiberreinforced cementitious composites," Cement and Concrete Composites, vol. 31, no. 4, pp. 232- 243.

28. F. Bayramov, C. Taşdemir, and M. Taşdemir, (2004). "Optimisation of steel fibre reinforced concretes by means of statistical response surface method," Cement and Concrete Composites, vol. 26, no. 6, pp. 665-675.